FOI-R--0875--SE
June 2003
ISSN 1650-1942
Base data report

Modeling of low-frequency sound propagation in the Baltic

Brodd Leif Andersson and Ilkka Karasalo

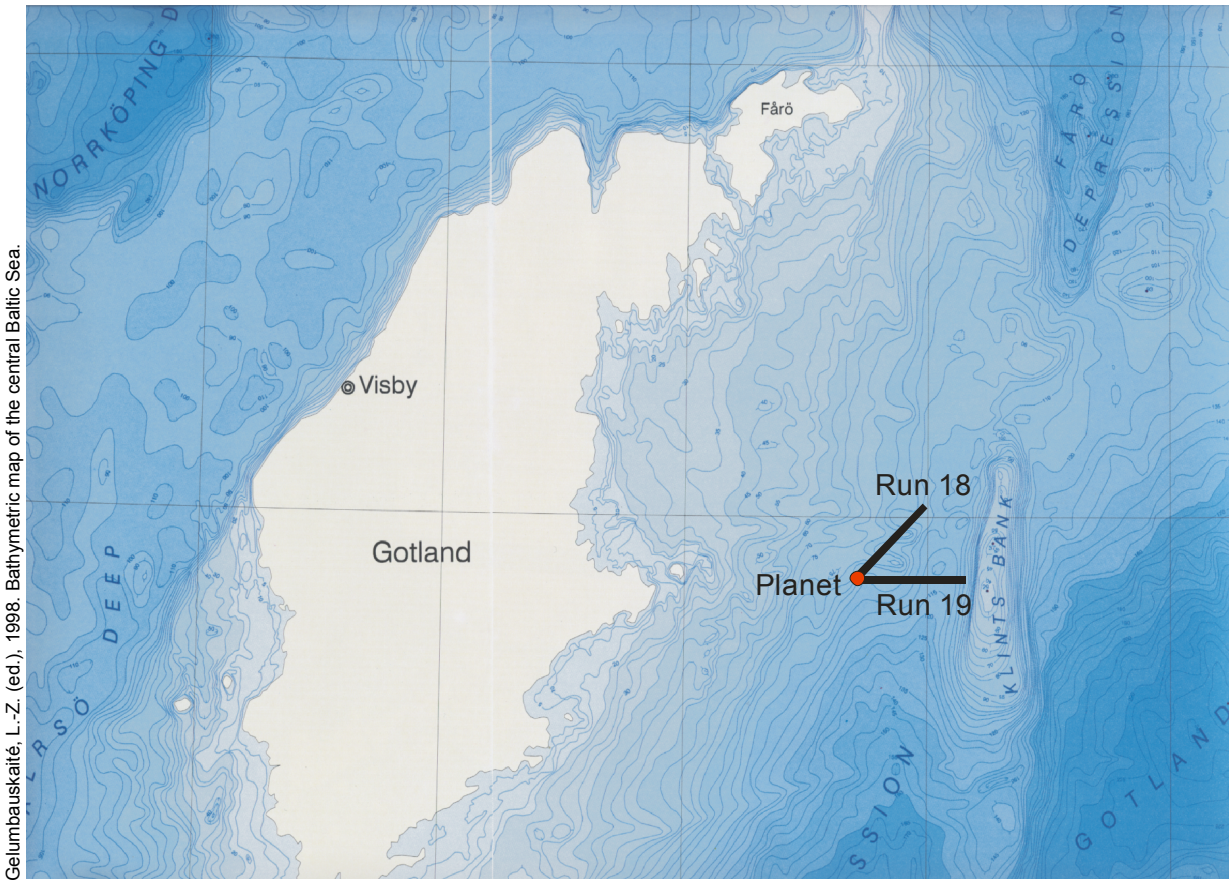

Gelumbauskaité, L.-Z. (ed.), 1998. Bathymetric map of the central Baltic Sea.

Systems Technology
SE-172 90 Stockholm

SWEDISH DEFENCE RESEARCH AGENCY

Systems Technology
SE-172 90 Stockholm

FOI-R--0875--SE

June 2003

ISSN 1650-1942

Base data report

Modeling of low-frequency sound propagation in the Baltic

Brodd Leif Andersson and Ilkka Karasalo

Issuing organization	Report number, ISRN	Report type
FOI – Swedish Defence Research Agency Systems Technology SE-172 90 Stockholm	FOI-R--0875--SE	Base data report
	Research area code 4. C4ISR	
	Month year June 2003	**Project no.** E6051
	Customers code 5. Commissioned Research	
	Sub area code 43 Underwater Sensors	

Author/s (editor/s)	Project manager
Brodd Leif Andersson Ilkka Karasalo	Peter Krylstedt
	Approved by Monica Dahlén
	Sponsoring agency Swedish Armed Forces
	Scientifically and technically responsible Ilkka Karasalo

Report title

Modeling of low-frequency sound propagation in the Baltic

Abstract (not more than 200 words)

Geoacoustic inversion techniques are applied on transmission loss (TL) data recorded in an area east of Gotland, to investigate how well the experimental data can be reproduced by a numerical sound propagation model. The data were recorded during the BAROC field trials performed by FOI and FWG in May 2002. The seabed parameters were estimated by minimizing the difference between simulated and experimental data with a genetic algorithm, using the parabolic wave equation as wave propagation model.

It is found that a range-independent fluid seabed model managed to reproduce the TL data with an accuracy of about 3 dB. Range-dependent modeling reduced the mismatch further by 1 dB. The models were of two fundamentally different types: Solid seabed with media parameters consistent with the knowledge of the geology in this area, and a fluid seabed with unrealistic parameters, in particular unrealistically low sound velocities in the sediment. The low sediment velocities seem to have compensated for losses caused by shear wave excitation in the solid model. Both types of models managed to reproduce the data with an accuracy of about 2 dB.

An example indicated that, if the absolute signal levels are not available, then matching of the relative decay rates in the TL data can be used as an alternative.

Keywords

Underwater acoustics, transmission loss, inversion, genetic algorithm, wave propagation model, sensitivity analysis, parabolic wave equation

Further bibliographic information	Language English
ISSN 1650-1942	**Pages** 62 p.
	Price acc. to pricelist

Utgivare	Rapportnummer, ISRN	Klassificering
Totalförsvarets Forskningsinstitut - FOI Systemteknik 172 90 Stockholm	FOI-R--0875--SE	Underlagsrapport
	Forskningsområde 4. Spaning och ledning	
	Månad, år Juni 2003	**Projektnummer** E6051
	Verksamhetsgren 5. Uppdragsfinansierad verksamhet	
	Delområde 43 Undervattenssensorer	

Författare/redaktör	Projektledare
Brodd Leif Andersson Ilkka Karasalo	Peter Krylstedt
	Godkänd av Monica Dahlén
	Uppdragsgivare/kundbeteckning Försvarsmakten
	Tekniskt och/eller vetenskapligt ansvarig Ilkka Karasalo

Rapportens titel (i översättning)

Modellering av lågfrekvent ljudutbredning i Östersjön

Sammanfattning (högst 200 ord)

Geoakustiska inversionstekniker har tillämpats på transmissionsförlustdata som har insamlats i ett område öster om Gotland för att undersöka hur väl experimentella data kan reproduceras av en numerisk ljudutbredningsmodell. Data insamlades under ett gemensamt fältförsök (BAROC) anordnat av FOI och FWG i maj 2002. Bottenparametrarna uppskattades genom att minimera skillnaden mellan modellberäknade och uppmätta värden med en genetisk algoritm, med den paraboliska vågekvationen som ljudutbredningsmodell.

Redan en avståndsoberoende fluid bottenmodell visade sig kunna återge data med en noggrannhet av ca 3 dB. Med avståndsberoende modellering kunde detta fel reduceras ytterligare med ca 1 dB. Modellerna var av två fundamentalt olika slag: Solid bottenmodell med mediaparametrar i närheten av de förväntade för denna typ av botten, samt fluid bottenmodell med mediaparametrar som kunde skilja sig markant från de förväntade, i synnerhet genom att hastigheterna i sedimentet blev orealistiskt låga. Dessa låga sedimenthastigheter tycks vara ett sätt för den fluida modellen att kompensera för förluster genom skjuvvågsexcitation. Båda typerna av modeller lyckades reproducera datakurvorna med en noggrannhet av ca 2 dB.

Ett exempel antydde att, om de absoluta signalnivåerna är okända, så kan anpassning mot det relativa avtagandet i data vara ett framkomligt alternativ i inversionssammanhang.

Nyckelord

Undervattensakustik, transmissionsförlust, inversion, genetisk algoritm, vågutbredningsmodell, känslighetsanalys, paraboliska vågekvationen

Övriga bibliografiska uppgifter	Språk Engelska
ISSN 1650-1942	**Antal sidor:** 62 s.
Distribution enligt missiv	**Pris: Enligt prislista**

Contents

1 Introduction

1.1 Background and purpose

In May 2002 a two-week hydroacoustic field trial was carried out in the Baltic, jointly by FOI and FWG (Forschungsanstalt der Bundeswehr für Wasserschall und Geophysik, Kiel, Germany). The purpose of the trial was to measure transmission loss, reverberation and time variability of the sound channel in areas with different seabed characteristics. Two test sites were chosen; the first close to Landsort, the second east of Gotland. At the Landsort site the seabed consists largely of exposed bedrock, at the Gotland site the seabed is softer, composed of 5-20 m sediments of clayey silt and moraine above limestone bedrock.

In this report we analyze a set of low-frequency transmission loss (TL) recordings from the Gotland site. The data consisted of CW-pulses at four frequencies in the range 30-120 Hz, and our objectives are, first, to investigate how well the data can be reproduced by numerical sound propagation models in which the parameters and geometry of the seabed are chosen optimally. Second, to compare the resulting 'acoustically equivalent' seabed model with prior geological knowledge of the seabed at the site. Differences between the estimated seabed model and geological 'ground truth' are inevitable, due to the comparatively simple structure of the model seabed, and to the limited amount of experimental data available. It is, however, worth stressing that such differences need not be harmful for the primary purpose of the equivalent seabed model, which is to predict the wave propagation in the water column in the frequency range covered by the experimental data.

A third objective is to investigate how sophisticated the environmental model needs to be in order to accurately reproduce the observed data. Is a range-independent fluid model enough, or must range dependence and/or shear wave excitation in the seabed be included ? The computational cost, both of finding an optimal model environment and of using the environment for TL predictions, increases with increasing model complexity. Choosing the simplest adequate model is therefore important in situations where a fast computational response is crucial, such as e.g. Rapid Environmental Assessment (REA) scenarios.

1.2 Geoacoustic inversion

For modeling acoustic propagation reliably in shallow water environments, knowledge of the properties of the seabed is required. Important seabed properties include bathymetry and geoacoustic parameters (density, compression and shear wave velocities and attenuations). Besides these parameters, knowledge about the sound velocity profile in the water is of utmost importance for producing high-quality model-predicted acoustic wavefields. While the water depth and sound velocity profiles in the water can be measured by fairly simple means, the seabed parameters are nearly impossible to determine in situ. Spotwise information of the geoacoustic parameters of the upper layers of the seabed can in principle be acquired by collecting core samples for subsequent

laboratory analysis. When densely sampled estimates of the parameters are needed in large areas, however, core sampling becomes impractically expensive and time consuming, and is, moreover, not likely to be applicable under operational conditions in hostile waters.

Geoacoustic inversion is a more economical way to acquire seabed information for sound propagation prediction. This means that a wave propagation code is run repeatedly for different choices of seabed parameters, and a search algorithm is used for finding combinations of these parameters that minimize the model-data mismatch. This optimization problem is highly non-linear, and the size of the multi-dimensional search space increases rapidly if the environmental model is allowed to vary with range.

In this work we have used the range-dependent Parabolic wave Equation (PE) model JEPE-S [1, 2] for computing the wavefields, and a genetic algorithm (GA) for searching optimal seabed parameters. Genetic algorithms need no derivative information and use random processes in the search for the global optimum. A characteristic of GA is that parameter values are represented by binary strings, collected to a single bit-string called a chromosome. These bitstrings are then manipulated in a manner which is analoguous to genetical evolution of biological systems to produce more successful, or better fit, organisms. An introduction to GA's is found in [3].

1.3 Summary of results

Referring to the objectives stated in Sec. 1.2, our results are, in summary:

First, the numerical sound propagation model JEPE-S managed to reproduce the experimentally observed transmission loss as function of range with an accuracy of about 2-3 dB for all four frequencies simultaneously.

Second, the range-dependent seabed models were of two different types: On one hand a solid seabed with parameters consistent with prior knowledge of the site, on the other a fluid seabed with unrealistic parameters, in particular unrealistically low sound speed in the sediment. Both models managed to reproduce the data. In fact, along the less lossy track 19 the simpler fluid seabed model gave the best match. The low sediment velocities of the fluid seabed model seem to have compensated for losses caused by shear wave excitation in the solid model. However, the solid seabed model is consistent with 'ground truth' and is therefore likely to produce more reliable predictions with respect to seasonal variations of the water level and the sound velocity profile.

Third, already the simplest model, a range-independent fluid seabed model, managed to reproduce the TL data with a mismatch of the order of 3 dB. This is not surprising since the seabed is almost flat at the site: The slope of the seabed nowhere exceeds one degree along the tracks. The range-dependent models reduced the mismatch further with up to 1 dB. In fact, further improvement of the match is not meaningful because of the uncertainties in the data.

The significance of shear wave excitation increases with increasing loss of sound into

the seabed: Along the lossy track 18 a fluid seabed model with realistic sound speed in the sediment gave about 2 dB larger mismatch than the solid seabed model, along the less lossy track 19 only about 0.5-1 dB larger.

The variations with range of the sound velocity in the water were small and had no effect on the wave propagation at these low frequencies.

An example indicated that, if the absolute signal levels were not available, then matching of the relative decay rates in the TL data can be used as an alternative.

2 The field trial

2.1 The test site

The bottom properties of the test site area east of Gotland exhibit no large variations. The water depth is about 100 metres and the seabed consists of a sediment of clayey silt and moraine above limestone bedrock. The thickness of the sediment varies between 5 and 20 metres. The density and sound velocity of the clayey silt layer is expected to be about 1200 kg/m^3 and 1600 m/s respectively, and that of the moraine layer 1800-2000 kg/m^3 and 1750-1800 m/s. For the limestone bedrock the corresponding values should be 2000 kg/m^3 and 3800-4000 m/s respectively [4, 5].

On May 14 2002, the last day of the field trial, TL-measurements were made along two tracks, one in the north-east direction from the receiving ship (Runs 17 and 18) and the other in the east direction (Run 19), see Fig. 2.1. Data from Runs 18 and 19 only are considered in this report.

The bathymetries and sound velocity profiles were continuously registered by echo sounder and a CTD-chain along the tracks, and the results are shown in Fig. 2.2.
We see that the CTD-chain, which consisted of about 80 sensors, did cover only the upper 50 metres of the water volume, and that the registrations were terminated after 6.8 km of Run 19. Single profiles were also registered at different locations and times during the day, and these show that the variations of the sound velocity profiles were modest, essentially all profiles show a linear decay from about 1450 m/s at the surface down to 1426 m/s at the axis of the sound channel between 60 and 70 metres depth, then increasing again to about 1440 m/s close to the bottom, see Fig. 2.3.

The variation of the water depth in Fig. 2.2 might look large, but this is an effect of the scaling of the axes. As a matter of fact the slope of the seabed nowhere exceeds one degree, i.e. the bottom is almost flat.

The weather conditions were perfect during the day of the trial. The wind speed was about 3-5 m/s and the wave height about 0.2 metres.

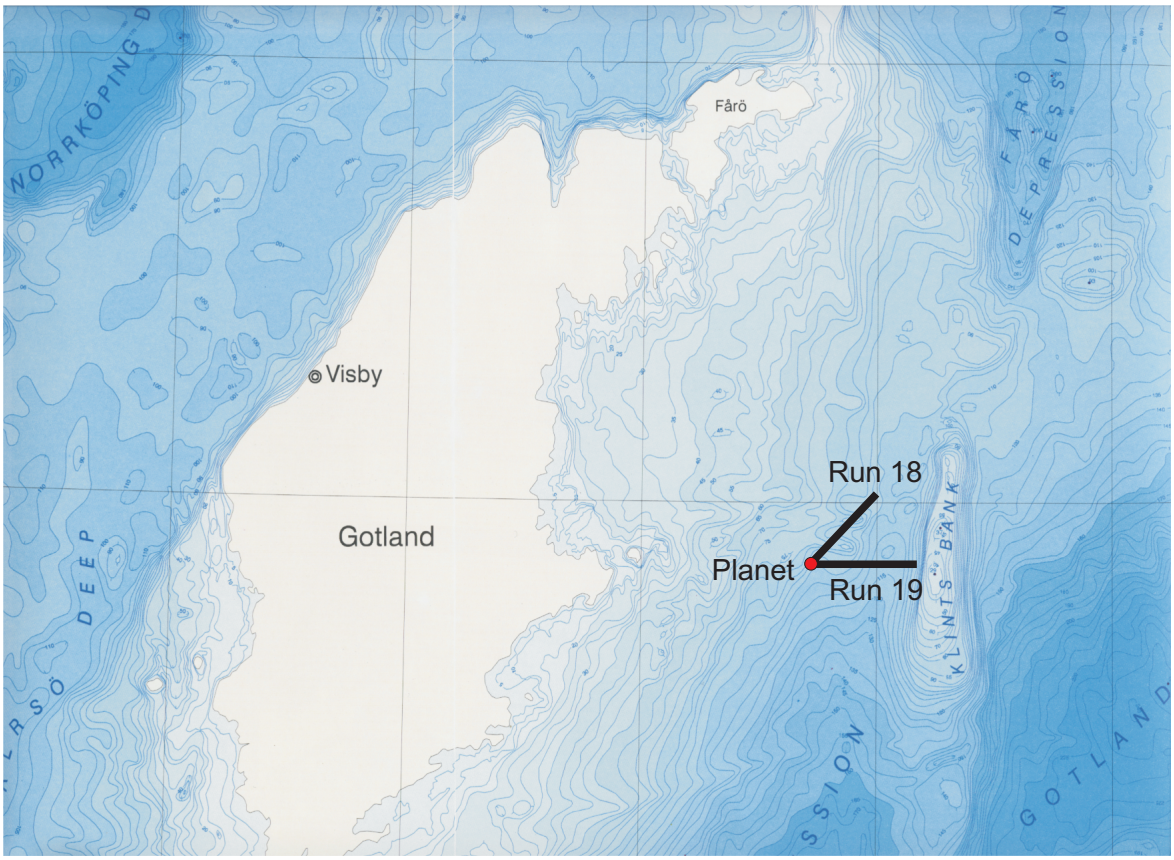

Figure 2.1: The test site at the TL-experiment on May 14 2002. (Map from Gelumbauskaité et al. 1998 [6]).

2.2 The experimental setup

Three different vessels were involved in the joint experiment: WFS Planet (Germany), MzB Schwedeneck (Germany) and HMS Urd (Sweden). All three vessels were equipped with GPS-synchronized trigger units for a common time scale and for synchronizing the data recordings.

WFS Planet was anchored at a fix position and served as a platform for the receiving systems during the TL measurements. A vertical array of 8 hydrophones was suspended from the ship, and the depths of the hydrophones were 10, 20, 30, 40, 50, 60, 70 and 90 metres respectively. The 4th (40 m) and 8th (90 m) didn't work, and the 3rd (30 m) was contaminated by noise. These three hydrophones were replaced by three others at the same depths but a few metres from the array. However, only the remaining five original hydrophones of the array are considered in the analysis below.

MzB Schwedeneck towed a hydraulic transducer which emitted CW-pulses in the range 30-120 Hz along two tracks: Run 17 was from and Run 18 towards WFS Planet along the north-east track, and Run 19 was from WFS Planet along the east track. Only Run 18 and Run 19 are considered in the analysis below. The speed of the ship was about

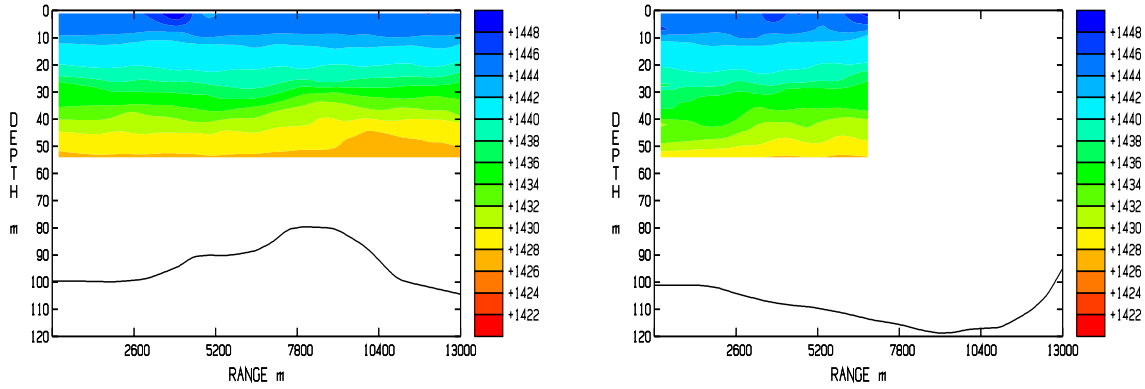

(a) Run 18

(b) Run 19

Figure 2.2: Bathymetries and measured sound velocities (m/s) during Runs 18 and 19 on May 14 2002.

4 knots, and the depths of the transmitter about 37 m (Run 18) and 55-60 m (Run 19). The bathymetry along the tracks and the position of the ship were continuously registered by echo sounder and GPS.

HMS Urd continuously registered CTD-profiles with a towed CTD-chain along the tracks in the close neighborhood of MzB Schewdeneck. Between the TL-runs it also measured single CTD-profiles (cfr. Figs. 2.2, 2.3).

2.3 Transmitted signals

Each 80 secs a trigger pulse (1 kHz CW-pulse of duration 0.05 secs) was transmitted from the platform vessel WFS Planet to MzB Schwedeneck by radio. This trigger pulse initiated the transmission of a train of four CW-pulses (30, 45, 70, 120 Hz), each of length 10 secs with 3 secs gap in between. The transmitted source levels were determined from the applied voltage via accelerometer sensitivity curves for the hydraulic transducer in dB rel 1V/μPa, see Tab. 2.1.

	Source level in dB rel 1 μPa at 1 m			
	30 Hz	45 Hz	70 Hz	120 Hz
Run 18	188.9	193.3	193.4	180.3
Run 19	188.3	192.7	193.1	180.3

Table 2.1: Source levels for the four CW-pulses in Runs 18 and 19.

3 Processing of the experimental data

The data were recorded with a sampling frequency of 8008 Hz and stored on files in a 15-channel frame with 16 bits/sample. The trigger-pulses and the position log-files

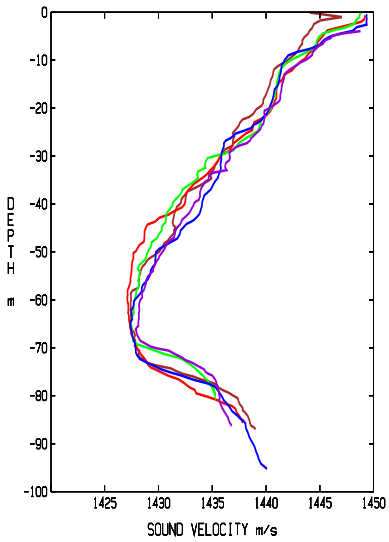

Figure 2.3: Sound velocity profiles measured at different locations and times in test site area 2 on May 14 2002.

of the transmitting vessel were used for estimating the travel times for the CW-pulses to the receiver array. When localized in this way, the power of the CW-pulses were computed by bandpass filtering.

3.1 Bandpass filtering

The bandpass filtering was done over the central 6 secs of the 10 secs long CW-pulses, this in order to safely embedd the filter windows within the signals. The transmitting vessel was moving about 12 metres during this time span (the speed was about 4 knots). Figure 3.1 shows the result of computing the sound pressure level (SPL) as function of distance to the transmitter in this way with three different choices of bandwidth in the bandpass filter.

We get an erroneous contribution to the signal if we choose a filter bandwidth larger than 1 Hz (red and green curves), while the blue curve (bandwidth 1 Hz) shows that the signal is actually lost in the ambient noise from about 7.5 km. The erroneous contribution seems to originate from the machinery of the receiving vessel, see Fig. 3.2.

The 30 Hz, 45 Hz and 70 Hz CW-pulses are easily recognizable from a distance of 2 km, while from 10 km they have disappeared in the background noise. The power-lines for 27.5 Hz, 46 Hz and 64.5 Hz are independent of the source-receiver separation and therefore probably emanate from the machinery of the receiving vessel. The sound pressure level (SPL) of these lines is about 115-120 dB rel 1 μPa. The 27.5 Hz and 64.5 Hz noise do not disturb the transmitted CW-pulses, and neither do the 46 Hz noise if we choose a filter bandwidth of 1 Hz centered around the frequency of the CW-pulse. Figure 3.3 shows the SPL of the received CW-pulses as function of source-receiver separation together with the corresponding ambient noise (average power of noise 10 secs before and after the CW-pulse).

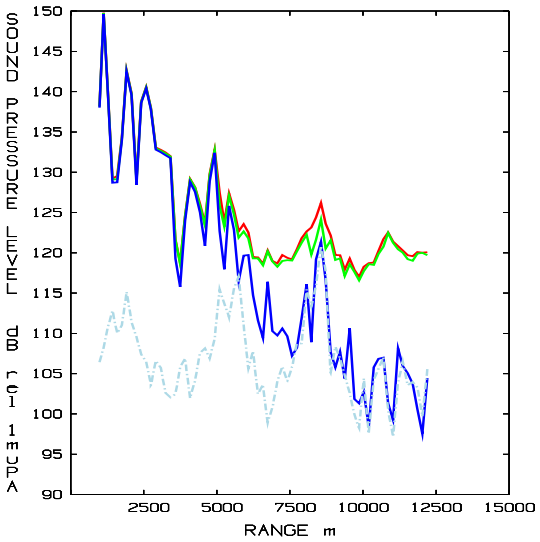

(a) 45 Hz, receiver depth 10 m, Run 18.

Figure 3.1: Sound pressure level as function of source-receiver separation computed by bandpass filtering with different choices of bandwidth: red (4 Hz), green (2 Hz) and blue (1 Hz). The light blue dashed line shows the ambient noise (1 Hz band).

We notice the quite different propagation characteristics between Run 18 and Run 19: in Run 18 the signals are lost in the background noise already after 5-7.5 km, while in Run 19 the signals are well above the ambient noise level still at the end of the run at 13 km. There is no obvious reason for this, the seabed is expected to be rather uniform in all directions at this test site [4]. A cause could be the different transmitter depths: In Run 18 the the source depth was about 37 m, in Run 19 the source was located near the center of the sound channel at about 60 m, cfr. Fig. 2.3. However, the model results show that this is not the reason since at these low frequencies the channel trapping effect is small. The reason is more likely to be local variations in the seabed: The seabed is softer along track 18 than along track 19.

We also notice the low signal strength of the 120 Hz data in both runs. This is ascribed to the comparatively low source level of this signal, cfr. Tab. 2.1.

The slow oscillation of the ambient noise curves are probably due to distant ship traffic, the test site was namely located close to a shippinglane. However, the increase in the ambient noise level at about 5-6 km and 11-13 km respectively at 30 Hz in Run 19 are at present not well understood. Here the noise level differs considerably between the different hydrophones in the array. Corresponding noise maxima are detected at the lowermost hydrophone at 45 Hz, while nothing is seen at 70 and 120 Hz. Similarly, the noise maxima at about 7 km at 70 and 120 Hz have no counterparts at 30 and 45 Hz, but at these maxima the noise level is the same in all hydrophones. The locations of the noise maxima in Run 18 are better correlated between the four frequencies.

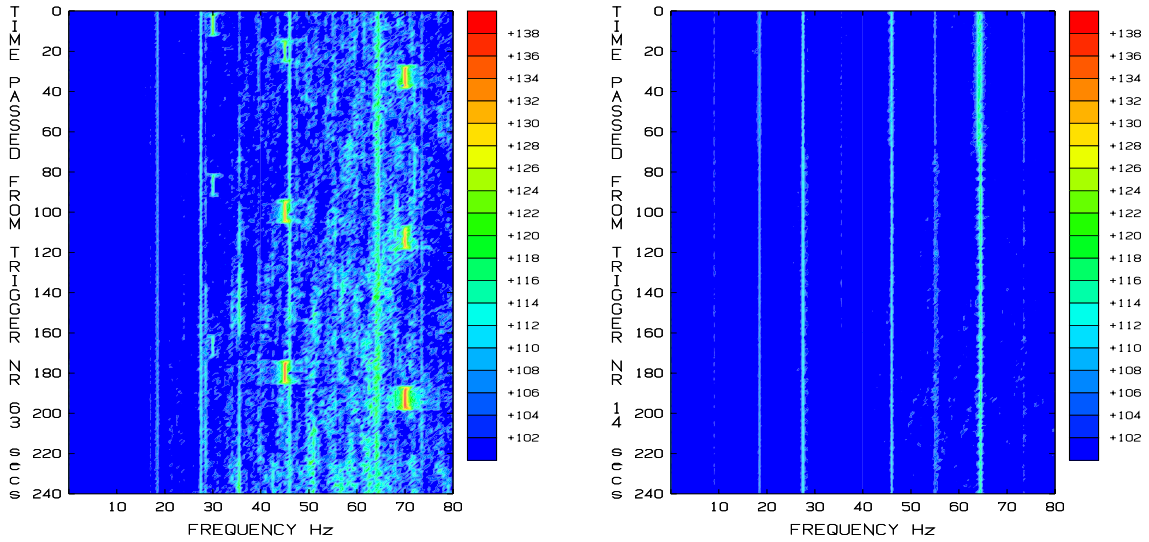

(a) Source-receiver separation about 2 km.

(b) Source-receiver separation about 10 km.

Figure 3.2: Power spectrum (dB rel 1 μPa) of the recorded data in the uppermost hydrophone at depth 10 m during two 4-minutes sessions of Run 18.

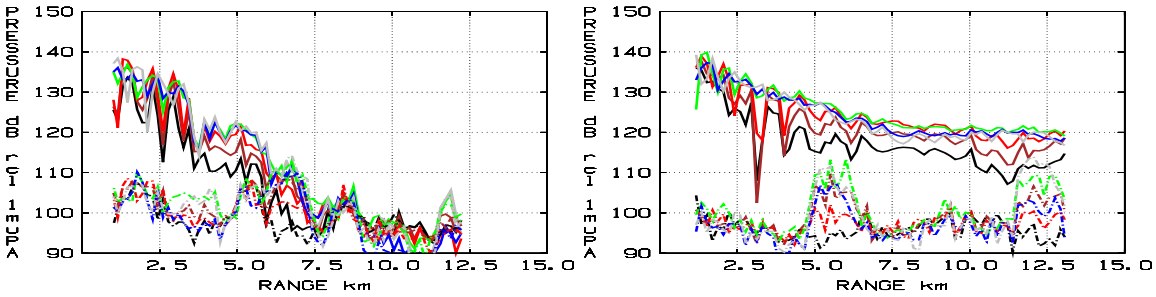

(a) 30 Hz, Run 18

(b) 30 Hz, Run 19

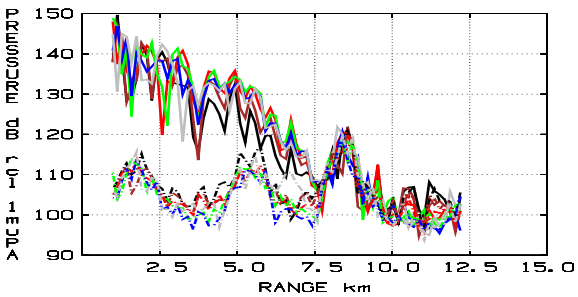

(c) 45 Hz, Run 18

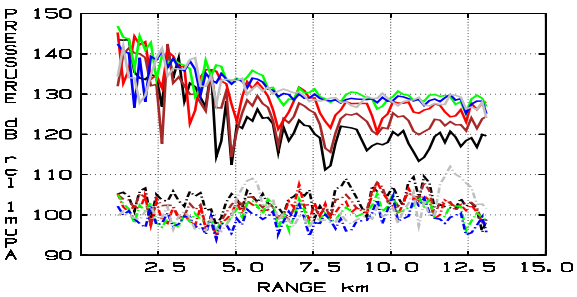

(d) 45 Hz, Run 19

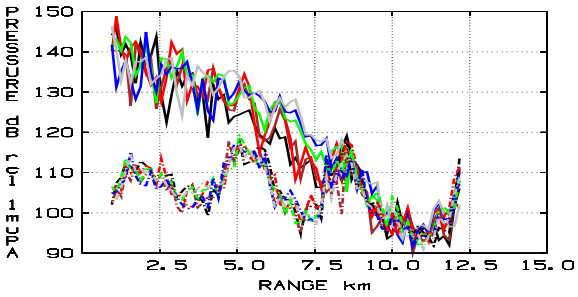

(e) 70 Hz, Run 18

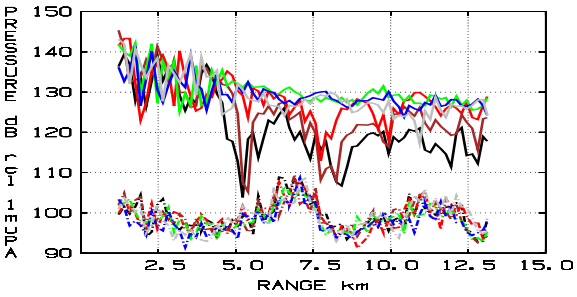

(f) 70 Hz, Run 19

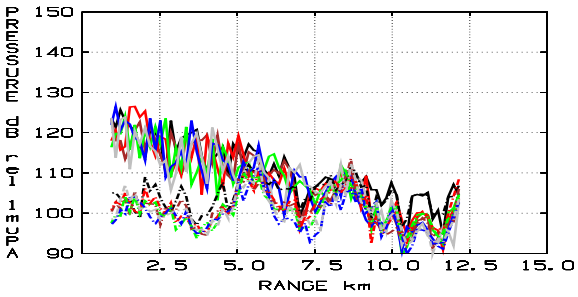

(g) 120 Hz, Run 18

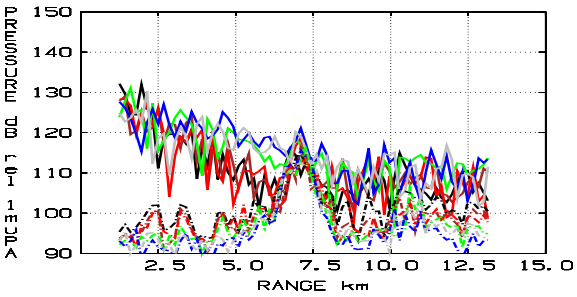

(h) 120 Hz, Run 19

Figure 3.3: Recorded sound pressure levels in dB rel 1 μPa as function of source-receiver separation (continuous lines) and ambient noise (dashed lines). Hydrophone depths are 10 m (black), 20 m (brown), 30 m (red), 50 m (green), 60 m (blue), 70 m (grey). The 3rd hydrophone (30 m, red lines) was reported to be contaminated by noise.

3.2 Preparation of data for inversion

The data in Fig. 3.3 are processed in two steps before they are ready to be used in an inversion scheme. First, data which lie too close to the ambient noise level (in our case within 10 dB) are removed from the data set. Second, the remaining data set is smoothed with a sliding rectangular window of length 1000 m. This is done in order to get rid of the large variations in data level in favour for a more pronounced trend in the TL-curves which hopefully could be matched by a wave propagation model. The process is illustrated in Fig. 3.4.

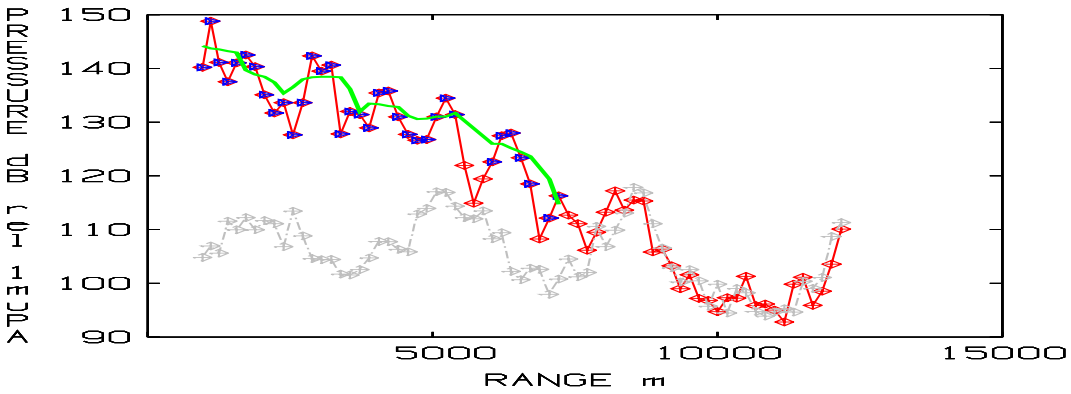

Figure 3.4: Pre-processing of the experimental data: The data (red) were compared with the ambient noise level (grey). Data points less than 10 dB above the noise level were removed. The remaining points (blue) were smoothed with a sliding rectangular window of length 1000 m. The resulting curve (green) was used as the target TL data in the inversion scheme. The model fields were smoothed in the same manner before matching against the data.

4 Modeling tools

The input to a wave propagation model is a description of the layer geometry and the associated acoustical parameters. The output is a computed pressure wave field that signifies the wave response of the given media to the signal source of the model. The basic idea of inverse modeling is to adjust the parameters of the model until a satisfactory fit between modeled and measured curves is achieved. This process is usually automated by using an optimization algorithm. In the present work a PE-model (Parabolic wave Equation model), JEPE-S, has been used as wave propagation model, and a genetic agorithm (GA) has been used for the optimization. The full field code XFEM was used for validation of the results for range-independent media.

4.1 JEPE-S

JEPE-S [1, 2] is a PE-model for wave propagation in slowly varying fluid/solid media in 2D which has been developed at FOI. It handles the forward part of the wave propagation within a limited angle sector (up to about 40 degrees relative the horizontal plane). The performance characteristics of the model therefore depends on the degree

of variability of the bottom topography: large variations imply high propagation angles and hence poorer accuracy of the computed wave fields. On the other hand, the model in general works well when the water depth varies slowly and the sound propagation therefore is almost horizontal. This is the case at the test site considered in this report (cfr. Fig. 2.2).

4.2 XFEM

XFEM computes the full wavefield from a mono-frequency source in a range-independent layered fluid-solid medium by a Hankel-Bessel transform integral method. It uses an adaptive high-order integration method for the transform integrals [7] and a node-free finite element technique based on exact finite elements [8] for solving the two-point boundary value problem for the field as function of depth at fixed horizontal wavenumber.

4.3 The Genetic Algorithm (GA)

A Genetic Algorithm (GA) for nonlinear stochastic optimization is based on the mechanisms of natural selection and natural genetics. The function which is to be optimized, the objective function, is defined on a discrete parameter space defined by the user. In accordance with established GA terminology, a point in the parameter space, in our case a set of geoacoustic parameters used for the computation of the objective function, is referred to as a model and the objective function is called the fitness function. An important ingredient in a GA is the binary encoding of models to chromosome-like binary strings. The GA takes an initial population of randomly selected models and manipulates it with the genetic operators of selection, crossover and mutation. GA's may differ in the way these three operators are implemented and applied.

Our GA is a minor modification of that used by Parastates in [9], which in turn was inspired mostly by the GENITOR II algorithm by Whitley and Starkweather [10]. It is a distributed GA, by which we mean that distinct subpopulations are introduced, on which separate genetic searches are made. However, at regular intervals a copy of the best individuals of each subpopulation is migrated to all other subpopulations, and a check is made that no individual occurs twice or more in these. In this way the distributed populations maintain some independence while at the same time sharing information.

5 Comments on the inversion scheme

In this section we present the generic environmental model which is to be matched against data. The search spaces of the geoacoustic parameters are presented together with the tuning parameters of the GA. We also give a brief account of possible error sources in the measured data and further uncertainties introduced when necessary simplifications are made in order to adapt the reality to the requirements of the propagation model.

5.1 Environmental model

The seabed at the test site is expected to consist of a 5-20 metres thick sediment of clayey silt and moraine above limestone bedrock [4]. We have tried to model this milieu with a 3-layer model consisting of a water-layer, one sediment-layer and a bedrock-layer. The thickness of the sediment is allowed to vary with range, the velocities (compressional and shear) of the sediment with both range and depth, and the densities and absorptions with range. Both the layer interfaces and the media parameters within each layer are smoothly varying with depth and range and are represented by splines of degree 5.

The conditions of the limestone bedrock were assumed to be known: density = 2000 kg/m^3, sound velocity = 4000 m/s and attenuation = 0.2 dB/λ. In the solid case we added the shear velocity = 2309 m/s and the shear attenuation 0.3 dB/λ.

5.2 Computational model

5.2.1 Vertical discretization

In the fluid inversions we have used a vertical discretization which was adapted for the highest frequency and the largest possible thickness of each layer. By introduction of an extra transparent interface in the bedrock at the depths 150 m (Run 18) and 170 m (Run 19) in order to prevent gridlines to intersect each other, we got a 4-layer model (the bottommost interface was located 10 wavelengths below the transparent interface). We used 200 vertical gridpoints in the water, 100 points in the sediment, and 50 plus 200 points in the bedrock which guaranteed that we had a resolution of at least 20 points/λ for vertical waves for all frequencies in the fluid inversion (in the range-independent 3-layer models the corresponding number of points was 200, 100 and 200 points respectively). The corresponding DAE-system (Differential Algebraic Equations) did thus consist of 550 rows, and the coefficient matrices were penta-diagonal[1].

A corresponding resolution of the shear waves should require a vertical discretization of 200 points in the water, 1000 points in the sediment (due to the possibility of a shear velocity of only 100 m/s), and 100 plus 400 points in the bedrock. Since we have to solve for both the compressional and shear parameters, we thus end up with a DAE-system consisting of 3200 rows and with coefficient matrices of bandwidth 11. In theory this results in an increase of the runtime for the solid inversion by a factor of about 20-25, in reality however, only with a factor of 6 since in the present form of JEPE-S the coefficient matrices are stored in 11-diagonal form whether the problem is fluid or not. However, it should be a rather straight-forward task to modify JEPE-S so that it takes advantage of the smaller bandwidth in fluid problems, thus increasing the runtimes of fluid problems with roughly a factor 4.

A resolution of 20 points/λ for waves propagating in the vertical direction is more than enough, that corresponds to about 30 points/λ for waves propagating within the angle interval supported by the model, i.e. 40 degrees relative to the horizontal. By reducing that resolution into halves we still get a very accurate model. We thus chose

200 points in the water, 500 in the sediment and 70 plus 200 in the bedrock in the solid seabed case, which amounts to a DAE-system consisting of 1740 rows, and a runtime exceeding that of the fluid problem with roughly a factor 3.

5.2.2 Horizontal discretization

The computational cost of any PE-implementation is dominated by the step by step integration in range. The integrator in JEPE-S is a multistep, second derivative, fourth-order accurate method by Jeltsch [11]. The scheme has been augmented by an automatic procedure to select the optimal stepsize so that a preset error criterion is fulfilled. Besides being cost-effective, it relieves the user from specifying the range step. We prescribed a minimum stepsize-length of $0.25 \cdot \lambda_{water}$.

5.3 Reciprocity

The TL-data were recorded at a vertical hydrophone array suspended from the receiveing platform vessel WFS Planet which was anchored at a fix position, while the source was towed at a slow speed by the vessel MzB Schwedeneck. However, the computational model requires a fixed source. This can be achieved by an exchange of source and receiver locations due to the reciprocity principle of linear acoustics [12]. The exchange is possible only for one receiver depth at a time. Thus, the cost for comparing the data and model fields is proportional to the product of the number of frequencies and the number of receiver depths.

In the case of range-independent media there is no need for exchanging source and receivers, one simply defines a coordinate system which moves with the source. In this way one can match the field at all hydrophones in a single run of the model. This, in combination with the fact that no grid-transformation needs to be computed, implies that range-independent model inversions are much faster than when the media are allowed to vary with range. Therefore, an important issue for REA (Rapid Environmental Assessment) is to evaluate when a horizontally stratified model is sufficiently accurate for the needs. When this is the case one should rather incorporate a normal mode (NM) propagation model instead of the range-marching PE-solver in the inversion scheme, since the runtimes of NM-models are independent of how far from the source one wants to compute the field.

5.4 Output range-grid

The model field is computed on the same range-grid as the TL-data. In order to in some extent mimic the process of the data processing (bandpass filtering of the signal over a 6 secs long time-window), the model field has been computed at 13 equidistant points centered ± 6 metres around each of the data range-grid points (the source was towed with a speed of 4 knots and hence covered about 12 metres during 6 secs). The model field was smoothed in the same way as the data before the matching took place.

5.5 The objective function

The objective function, which gives a quantitative measure of the model-data mismatch, is defined as the mean l_2-norm of the difference between the model and data dB-values for all frequencies, receiver depths and ranges.

An alternative way to estimate the model-data mismatch when data are not calibrated is to approximate the difference $(\mathbf{TL}_{data} - \mathbf{TL}_{model})$ with a horizontal line in the least squares sense, where $\mathbf{TL}_{data}$ and $\mathbf{TL}_{model}$ are the measured and modeled dB-values respectively. This means that one solves for a γ which minimizes $\|\mathbf{TL}_{data} - \mathbf{TL}_{model} - \gamma \cdot \mathbf{1}\|_2$. Minimum is attained for $\hat{\gamma} = \frac{1}{M}\sum_{m=1}^{M}(\mathbf{TL}_{data}(m) - \mathbf{TL}_{model}(m))$, where M is the number of observations. The alternative objective function is thus given by $\frac{1}{\sqrt{M}}\|\mathbf{TL}_{data} - \mathbf{TL}_{model} - \hat{\gamma} \cdot \mathbf{1}\|_2$, i.e. the simulated transmission loss has been translated to favour a matching of the shape of the data to the expense of the absolute level. This is illustrated in Fig. 5.1.

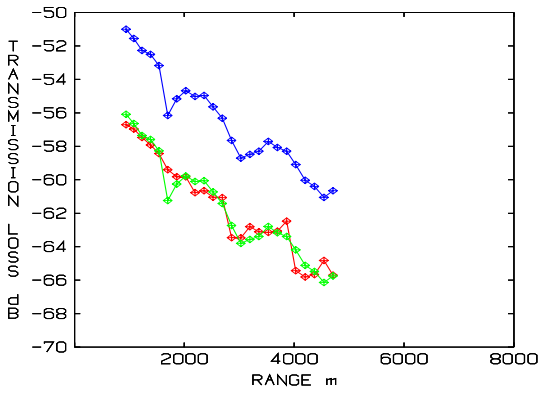

Figure 5.1: Data (red), model (blue, fitness=5.14) and vertically translated model (green, fitness = 0.69).

In inversions 18:2 and 18:2B in Sec. 7 both versions of the objective function are used in order to get an idea of how the result of the inversion is influenced of the type of fitness evaluation. In the remaining inversions the first version relying on calibrated values are used.

5.6 The search spaces of the geoacoustic parameters

The search intervals for the geoacoustic parameters in each of the inversions are tabulated in Tab. 5.1. The range points at which they were sought are presented in Sec. 6 together with supplementary details about the inversions. At each range point the compression and shear wave velocities were allowed to vary linearly with depth. c_p^{top} and c_p^{bot} denote the p-velocities at the upper and lower interface of the sediment, similarly for the s-velocities. ρ, β_p and β_s denote the density and the compression and shear attenuations respectively of the sediment.

Parameter	Run 18			
	Inversion 18:1	Inversion 18:2	Inversion 18:3	Inversion 18:4
Water depth [m]	80 - 100 (6)	•	•	•
c_p^{top} [m/s]	1100 - 2200 (6)	1100 - 2200 (6)	1550 - 1750 (6)	1550 - 1750 (6)
$\partial c_p/\partial z$ [1/s]	0 - 25 (4)	0 - 25 (4)	0 - 25 (4)	0 - 25 (4)
c_s^{top} [m/s]	•	•	•	100 - 600 (5)
$\partial c_s/\partial z$ [1/s]	•	•	•	0 - 10 (4)
β_p [dB/λ]	0.1 - 2.0 (4)	0.1 - 2.0 (4)	0.1 - 1.3 (4)	0.1 - 1.3 (4)
β_s [dB/λ]	•	•	•	0.0 - 2.0 (4)
ρ [kg/m^3]	800 - 2200 (4)	800 - 2200 (4)	1000 - 2000 (4)	1000 - 2000 (4)
Thickness [m]	2 - 40 (5)	2 - 40 (5)	2 - 40 (5)	2 - 40 (5)

Table 5.1: The parameter search intervals in the inversions on Run 18. The number of bits used in the discretization of each parameter is given within paranthesis. The search space for the inversions on Run 19 is identical apart from the water depth: $[90, 120]$ is used there.

5.7 GA-parameters

There are a number of parameters which can be used to "tune" the GA. We have used 6 populations with 1000 individuals in each and 350 model evaluations/population before migration took place, at which the 3 best individuals of each population were migrated to the other populations. The ranking function $y = x^3$ was used in the parent selection phase of the GA: $y = x$ will give no preference for any parents, while increasing powers of x increase the probability for choosing a parent with better fitness value. However, the risk of getting caught in a local minimum of the objective function also increases with increasing powers of x.

Depending on the complexity of the problem, up to 40 migrations were done which amounts to 92100 model evaluations. Each evaluation of a range-dependent model consists of $N_{freq} \times M_{Hyd}$ runs of JEPE-S, where N_{freq} and M_{Hyd} denote the number of frequencies and hydrophones respectively. This requires a large amount of computer resources. The GA has therefore been implemented on a Linux-cluster consisting of 20 nodes. The runtime for the range-independent fluid inversion 18:1 (92100 model evaluations) was about 10 hours, while that of the range-dependent solid inversion 18:4 (was terminated after about 30000 model evaluations) was about 7 days.

5.8 Uncertainties in experimental data

The sound level of the recorded data was determined by visual inspection of the calibration curves for each of the hydrophones in the array. We made a simplification by replacing the individual values of each hydrophone with an average over the hydrophones at each frequency. This resulted in the sensitivity values (dB rel 1 V/μPa) shown in Tab. 5.2. It should be noted that the gain of the preamplifier (=30 dB) is included in these values.

A reason for not using the individual sensitivity values for each hydrophone is the further uncertainties introduced due to the conditions at the test site: the calibration was

Frequency	30 Hz	45 Hz	70 Hz	120 Hz
Sensitivity [dB rel 1 V/μPa]	-166.25 ± 0.75	-166 ± 0.5	-164.5 ± 1	-164 ± 0.5

Table 5.2: The average sensitivity of the hydrophones in the receiver array.

done at a temperature of 20^oC, while the temperature at the test site varied between 3 and 8^oC, see Fig. 5.2.

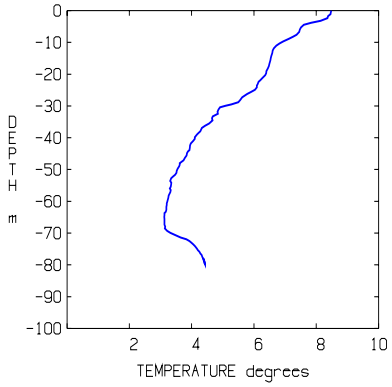

Figure 5.2: Typical temperature profile at test site 2 on May 14 2002.

In summary, the uncertainties in the experimental data due to the calibration of the hydrophones were estimated to be of the order of ± 1 dB.

5.9 Uncertainties due to model requirements

The position of the receiving platform WFS Planet was not perfectly fixed during the experiment, but was drifting up to ± 100 metres around an average postion, mainly in the east-west direction, see Fig. 5.3.

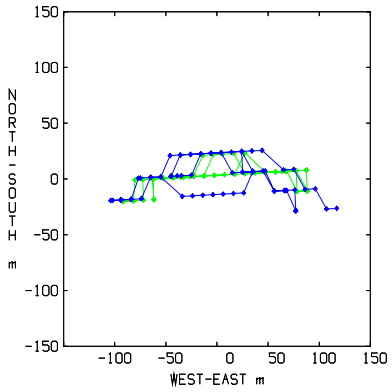

Figure 5.3: Drifting of the receiver platform vessel WFS Planet around the respective average positions during Run 18 (green) and Run 19 (blue) on May 14 2002.

However, JEPE-S requires a fixed source (source and receiver exchanged due to reciprocity). We have chosen the average position during each of the runs. The effect of

this approximation becomes more pronounced the smaller the distance between the source and receiver. By this reason we decided to match the data and model fields at source-receiver separations no smaller than 1 km. At this separation, assuming a decay between cylindrical and spherical, an uncertainty in position of about ±100 metres implies a corresponding uncertainty in the sound level of at most ±1 dB. Hence, the uncertainty in the model-data mismatch due to the approximation of a fixed source located at the average position during the measurements should be well below ±1 dB.

Another possible source of uncertainty is the depth of the transmitter, which corresponds to the depth of the receiver in the model due to reciprocity. In the present form of JEPE-S the receiver points must be defined on a cartesian grid, and it is thus not possible to model the variability of the source depth, cfr. Fig 5.4. The variation is about ±2 metres around the average depth. The effect of this variation on the recorded data is expected to be low at the low frequencies considered here.

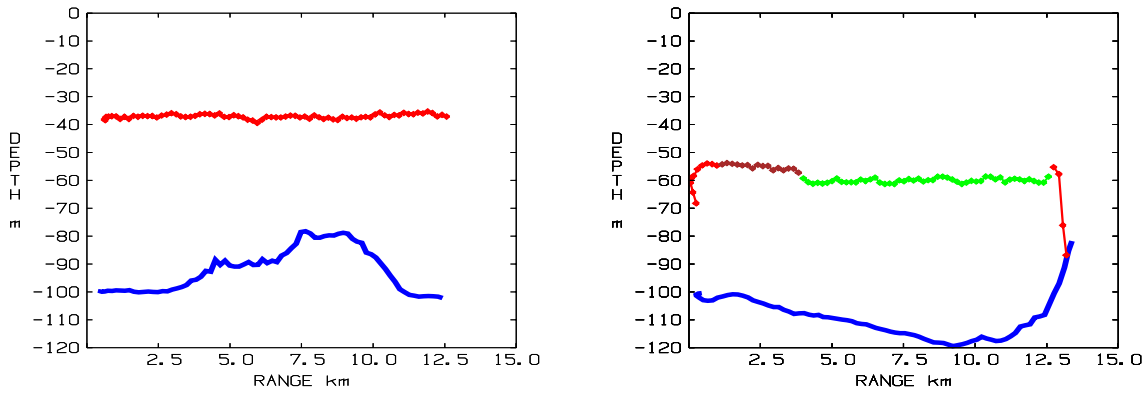

(a) Run 18

(b) Run 19

Figure 5.4: The bathymetries (blue) and the depths of the transmitter in Runs 18 (red) and 19 (red, brown, green and red) on May 14 2002. Obviously something happened at the end of Run 19.

The average depth of the transmitter in Run 18 was 37.0 m. The brown and green parts of the transmitter depth in Run 19 denote regions of different average depths: the average depth of the transmitter in the brown part is 55.0 m, in the green part 60.1 m. These different average depths were taken into account in the inversions.

Finally, uncertainties are introduced due to approximations done in the model itself: The source, for example, is approximated with a truncated mode basis corresponding to propagating modes within a limited elevation angle interval. The seabed is approximated by a sediment layer with smoothly varying geoacoustic parameters, thus neglecting inevitable inhomogenieties.

All together, the error sources discussed in these last two subsections will most likely introduce an uncertainty of about ±2-3 dB in the data used in the inversions.

5.10 Uncertainties due to sparse data sampling

An additional source of errors in the inversions, not of less importance than those described above, is that the data were recorded in short time intervals with a large separation in range. The data were recorded on range-grids with a stepsize of about 150-200 m, while the wavelengths for the frequencies in the analysis are about 10-50 m. The smoothed data curves used in the inversions therefore become extremely sensitive to the location of the individual datapoints: the TL-curves can differ several dB depending on if the data are located close to local minima or maxima of the interference patterns. This is illustrated in Fig. 5.5. By slightly translating the sparse output range-grids some 10 metres one gets TL-curves which differ up to 6-7 dB in this case. One way to reduce this uncertainty could be to use longer recording intervals for the low-frequency data, say, a few wavelengths in range.

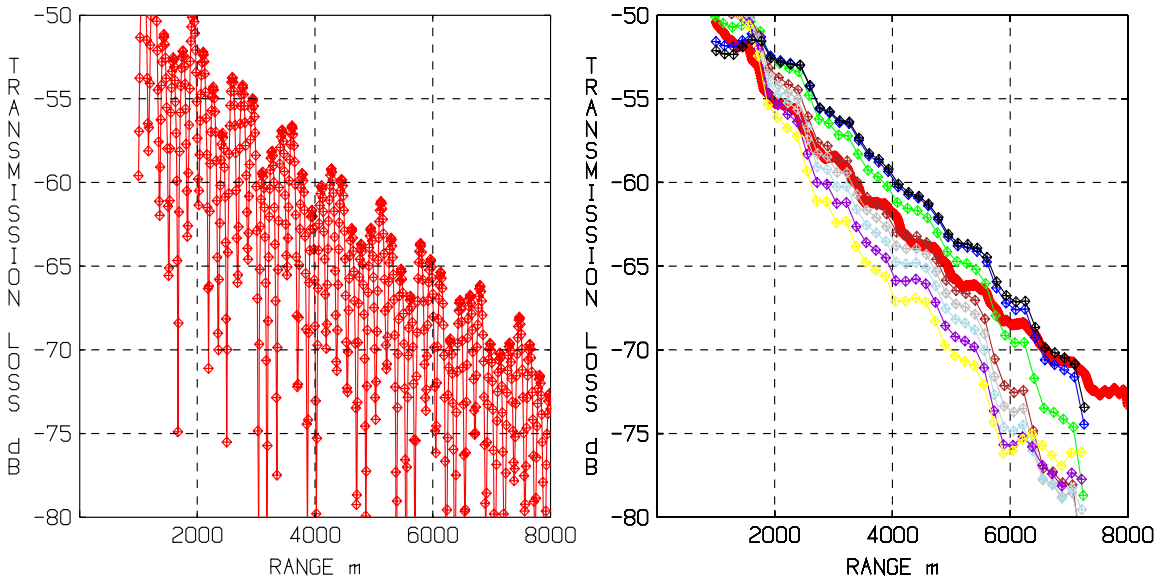

(a) Original unsmoothed solution computed by JEPE-S on a dense range-grid.

(b) Smoothed solutions computed by JEPE-S on a dense range-grid (red) and on sparse range-grids which are slightly translated w.r.t. each other.

Figure 5.5: Modelled TL-curves illustrating the effect of too sparse sampling of the data. The medium is obtained from inversion 18:1. The frequency was 45 Hz, and the receiver depth 60 m. Left: Densely sampled TL-curve obtained from JEPE-S. Right: Smoothed TL-curves for the dense range-grid (red) and for the data range-grid used in the inversion (green). The other smoothed curves are computed on range-grids which are slightly translated w.r.t. the data grid: black (+20 m), blue (+15 m), brown (-15 m), grey (-20 m), ligth blue (-25 m), dark violet (-30 m) and yellow (-35 m). The TL-curves are thus very sensitive for the locations of the individual data points when the data grid is sparse.

6 Supplementary details about the inversions

In this section we summarize details about the inversions like for example which data set has been used, which control data set to assess the inversion results and the number of model evaluations done.

6.1 Inversion cases

In all, eight inversion cases were studied, four on each of Runs 18 and 19. The cases are characterized by the assumed geometry (dependent/independent of range), seabed material type (fluid/solid), and the value intervals allowed for search of optimal seabed parameters (unrealistic values excluded/allowed). They are numbered 18:1, ..., 19:4, and are as shown in Tab. 6.1.

Case number	Geometry	Seabed material	Search interval
18:1, 19:1	range-independent	fluid	unrealistic
18:2, 19:2	range-dependent	fluid	unrealistic
18:3, 19:3	range-dependent	fluid	realistic
18:4, 19:4	range-dependent	solid	realistic

Table 6.1: Inversion cases.

In the realistic search intervals, the parameter values are restricted to be close to the expected ground truth, cfr. Tab. 5.1. The unrealistic intervals extend to values far away from ground truth, allowing, in particular, the sound speed in fluid sediments to be much lower than that in water. We remark that such low sound speeds would in fact be realistic if the sediment was gassy, however the gas content of the sediments at the site is expected to be insignificant.

In the :1 and :2 cases the search intervals of the geoacoustic parameters were deliberately chosen very large to find out if the inversion would result in parameter values close to the expected ground truth, cfr. Tab. 5.1. The sound speed in the seabed obtained in this way turned out to be unrealistically low, however, especially for the fast-decaying data set of Run 18.

Then, to investigate whether this was an effect of the GA being trapped in a local minimum, or if a minimum for higher velocities did actually not exist, the :3 cases were run, with search spaces close to the expected ground truth. In these cases, the good matchings of 18:2 and 19:2 could not be reproduced, in particuler 18:3 was considerably worse than 18:2.

Finally, in inversions 18:4 and 19:4 shear parameters were introduced to the realistic parameter search intervals of 18:3 and 19:3. The matches obtained with this solid seabed model were almost as good as those of the :2 cases, presumably by shear wave excitation replacing the low compressional sound speed as a mechanism for strong acoustic coupling beween the water column and the seabed.

All eight inversions were done on calibrated data, i.e. the absolute level of the data were taken into account. To get an idea of how the result of the inversion depends

on the type of fitness evaluation an extra inversion (18:2B) was performed where the model curves were vertically translated to fit the shapes of the data curves, cfr. Sec. 5.5. The resulting media model was roughly consistent with that of 18:2.

6.2 Inversion range points

The range points for the unknown media parameters of the range-dependent models were chosen to 1.0, 2.5, 3.5, 4.5, 6.0 and 8.0 km for Run 18 and 1, 2, 4, 5, 6, 8, 9, 11 and 13 km for Run 19. Outside these ranges the parameters were defined by linear interpolation and by fitting variance reducing splines of degree 5.

6.3 Size of search spaces

The size of the multi-dimensional search space increases rapidly if the environmental model is allowed to vary with range. In Tab. 5.1 the number of bits used in the discretization of each parameter is given within paranthesis. If we sum up the number of bits in the parameters of the range-independent inversion 18:1, we get a total of 29 bits which represents 6 parameters. This implies that the search space consists of $2^{29} = 5.4 \times 10^8$ points (or models). The size of the search spaces for all inversions are shown in Tab. 6.2.

Case nr	Seabed	Nr params	Nr bits	Search space size
18:1	rangeind fluid	6	29	5.4×10^{8}
18:2	rangedep fluid	30	138	3.5×10^{41}
18:2B	rangedep fluid	30	138	3.5×10^{41}
18:3	rangedep fluid	30	138	3.5×10^{41}
18:4	rangedep solid	48	216	1.1×10^{65}
19:1	rangeind fluid	6	29	5.4×10^{8}
19:2	rangedep fluid	45	207	2.1×10^{62}
19:3	rangedep fluid	45	207	2.1×10^{62}
19:4	rangedep solid	72	324	3.4×10^{97}

Table 6.2: Number of sought parameters and number of points (models) in the search spaces of the inversions.

We note the rapid increase in the size of the search spaces when media are allowed to vary with range. The number of parameters sought for (and hence the size of the search space) could be reduced by prior analysis of which parameters have a negligible influence on the transmission loss and simply omitting these insignificant parameters from the inversion. This has not been done in the present work, all geoacoustic parameters have been sought for.

6.4 Fitness values and number of model evaluations

The fitness values of the inversion models and the number of model evaluations together with the model evaluation at which the last improvement of the fitness value

occured are shown in Tab. 6.3.

Inversion	Seabed	Nr model evaluations	Last improvement	Fitness value
18:1	rangeind fluid	92100	38961	2.78
18:2	rangedep fluid	36449	35654	1.98
18:2B	rangedep fluid	50100	49048	1.49*
18:3	rangedep fluid	50100	38411	4.14
18:4	rangedep solid	31200	29705	2.27
19:1	rangeind fluid	43100	14693	2.84
19:2	rangedep fluid	41700	39593	1.97
19:3	rangedep fluid	37150	36040	3.16
19:4	rangedep solid	24305	22922	2.62

Table 6.3: Number of model evaluations, the model evaluation at which the last improvement of the fitness value occured, and the best fitness value of each inversion. Note that in the evaluation of the fitness values in inversion 18:2B account has not been taken for the absolute level of the data, the model curves have been translated to fit the shapes of the data curves, cfr. Sec. 5.5.

6.5 Inversion data set

The available data were TL as function of range for four frequencies and six receiver depths. All four frequencies (30, 45, 70, 120 Hz) and the two receiver depths 20 and 60 m were used in the inversions. Range-independent sound velocity profiles were used by choosing the one which was registered in the immediate neighborhood of the run of interest in Fig. 2.3.

6.6 Control data set

The TL-curves from the remaining four receiver-depths (10, 30, 50, 70 m) were used as control data. It should be remembered that the hydrophone on depth 30 m was reported to be contaminated by noise. Therefore we divided the control data set in two parts: control data set 1 contained the TL-curves for receiver depths 10, 50 and 70 m, control data set 2 the (maybe contaminated) TL-curves for receiver depth 30 m.

6.7 Sensitivity analysis

The aim of sensitivity analysis is to get an idea about the degree of influence of different seabed parameters on the transmission loss. In Secs. 7.5 and 8.4 we present such sensitivity analyses on the media obtained from the range-independent fluid inversions 18:1 and 19:1. Variations of the sound velocity profile with range in the water, and varying transmitter depths are discussed for the fluid range-dependent model 18:2 in Sec. 7.3.

7 Inversion results: Run 18

In this and the next section we present the results of the inversions. This section contains the results from the inversions on data from Run 18, and Sec. 8 the corresponding results from Run 19.

According to the discussion at the end of Sec. 5 the uncertainties in the data are of the order 2 to 3 dB. Hence, better agreement between data and model than this is not meaningful. As seen in Fig. 3.3, the propagation characteristics along the two runs are quite different. Along track 18 the transmission loss is of the order 40 dB/decade, which indicates that the seabed is soft and highly absorptive. Along track 19 the transmission loss is roughly 20 dB/decade, indicating a hard bottom making losses by absorption in the seabed very small. These characteristics of the seabed should be reflected in the inversion results below.

According to the knowledge about the geology at the test site, the seabed consists of sediments of clayey silt and moraine above limestone bedrock. The total thickness of the sediments is expected to vary between 5 and 20 metres. The density and sound velocity of the clayey silt layer should be about 1200 kg/m^3 and 1600 m/s respectively, and that of the moraine layer 1800-2000 kg/m^3 and 1750-1800 m/s. For the limestone bedrock the corresponding values are 2000 kg/m^3 and 3800-4000 m/s respectively [4, 5].

Of the investigated models the solid seabed model is the most advanced. It results in good matching of the data with seabed parameters which are close to the expected ground truth. The range-dependent fluid seabed model 18:2 gave as good matching (Sec. 7.3), but at the expense of unrealistically low velocities of the seabed. In fact, seabed velocities below the velocity of the water have been observed at an earlier field trial in the Stockholm archipelago [13]. There the parameters of the seabed were found by travel time analysis of transmitted Ricker-pulses in the frequency range 0.5-4 km, indicating a velocity at the seafloor of 1390 m/s. The low velocities in the present fluid model (down to 1100 m/s) seem to be a way for the fluid model to compensate for the absence of loss-mechanisms due to shear waves.

In the case of the range-dependent fluid model obtained from inversion 18:2 in Sec. 7.3, the inversion was repeated using a fitness function independent of the absolute level of the data (Sec. 7.4). The media model obtained was rather consistent with that of the original fitness function, which indicates that this type of inversion is a good alternative when source and/or receivers are not well calibrated or the wave propagation model by some reason has difficulties to compute the correct sound level, as can be the case for PE-models at very low frequencies, shallow depths and thin sediments.

We begin with the result for the most complex model, that is, the range-dependent solid seabed model (Sec. 7.1), and gradually reduce the complexity down to a horizontally stratified fluid seabed model (Sec. 7.5). Sensitivity analysis is confined to the least complex model.

7.1 Range-dependent solid seabed: Inversion 18:4

See Tab. 5.1 for the search-intervals of the geoacoustic parameters. The resulting medium is shown in Figs. 7.1 and 7.2. The fitness values for the inversion data set and the control data sets are shown in Tab. 7.1, and Fig. 7.3 shows the agreement between the experimentally observed TL curves and the model.

Except for the very beginning of the track, the thickness of the sediment layer agrees well with that expected from a geological point of view (5-20 m), and the compressional wave velocity and density also agrees well with the expected ground truth. The model field adapts well to the data except for 120 Hz. We notice the strange behaviour of the data at this frequency: the sound level is almost constant between 1 and 3 km at depth 20 m and quite low at both depths, about -60 dB. This could be an effect of the sparse sampling of the data points, cfr. Sec. 5.10. It turned out that all inverted models, regardless of the degree of complexity, had difficulties to match this behaviour.

As is well known, the elastic parameters of physically realizable solid media must be such that the strain energy as function of displacement is positive definite everywhere [14, Sec. 12.6]. This condition implies that the Lamé parameters λ and μ of the medium [15, Sec. 2.2] must be such that $\lambda + 2\mu/3$ (the bulk modulus) at all points of the medium lies in the fourth quadrant of the complex plane. We remark that although this condition was ignored during the GA search, subsequent numerical checks showed it to be satisfied for the resulting optimal solid seabed model.

	Fitness [dB]		
Frequency [Hz]	Inversion data set	Control data set 1	Control data set 2
30	1.81	2.19	2.16
45	1.76	3.44	1.37
70	2.10	2.81	2.49
120	3.46	4.21	4.43
All 4 frequencies	2.27	3.16	2.65

Table 7.1: Inversion case 18:4. Fitness values for the inversion data set (receiver depths 20 and 60 m), control data set 1 (receiver depths 10, 50 and 70 m) and control data set 2 (receiver depth 30 m, maybe contaminated by noise, cfr. Sec. 6.6.). Cfr. Tab. 7.2.

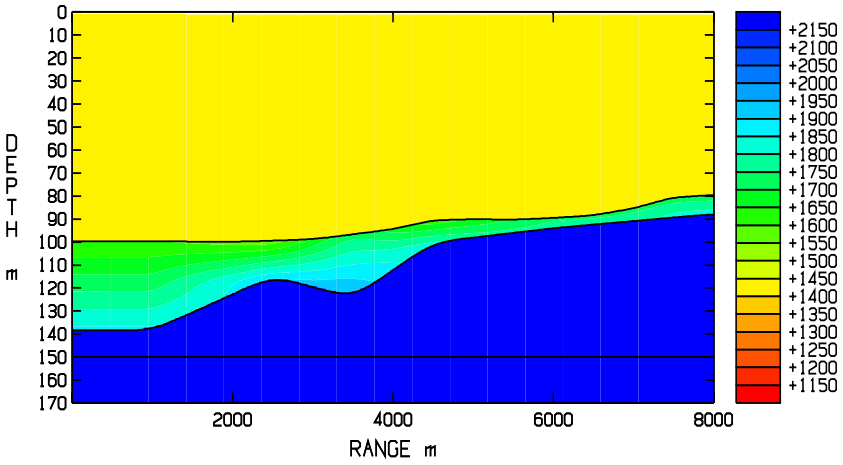

(a) P-velocity (m/s)

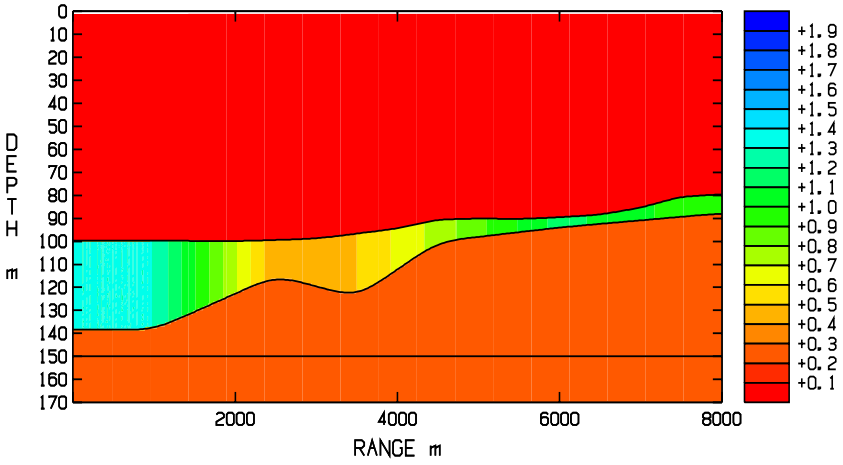

(b) P-attenuation (dB/λ)

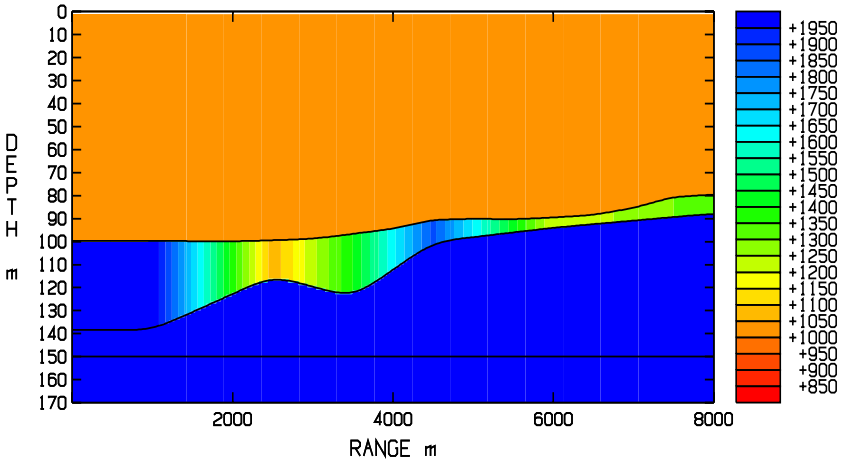

(c) Density (kg/m^3)

Figure 7.1: Media parameters obtained from inversion 18:4.

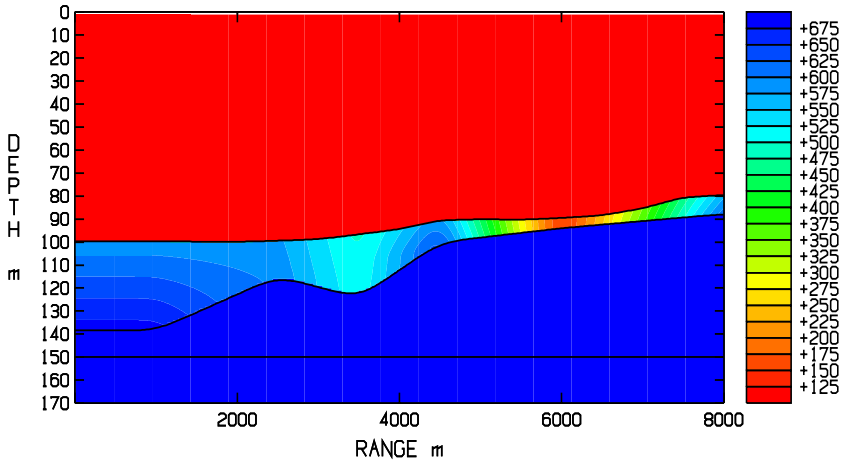

(a) S-velocity (m/s)

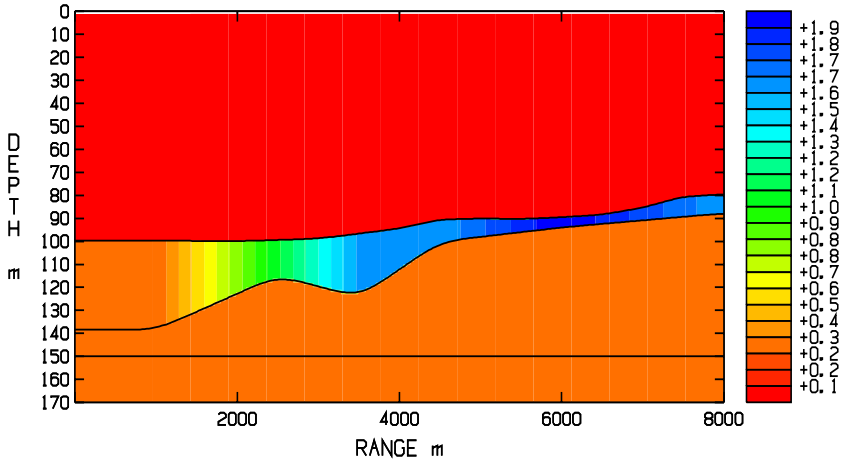

(b) S-attenuation (dB/λ)

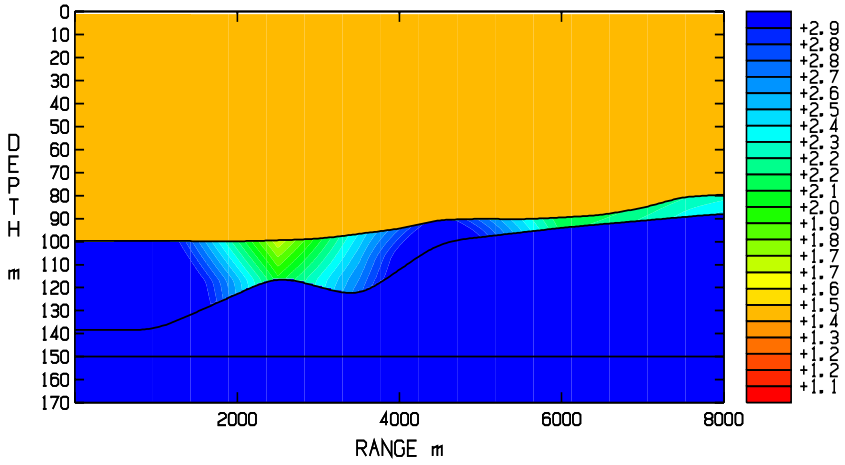

(c) The acoustic impedance (10^6 kg/m^{2}s)

Figure 7.2: Shear parameters and acoustic impedance obtained from inversion 18:4.

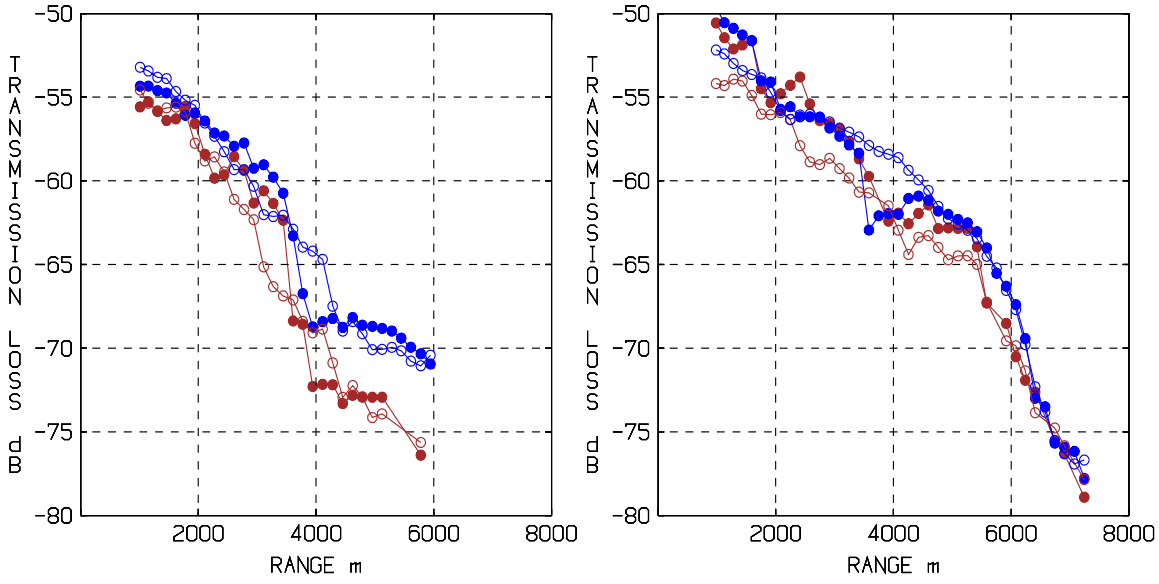

(a) 30 Hz, Fitness = 1.81 dB

(b) 45 Hz, Fitness = 1.76 dB

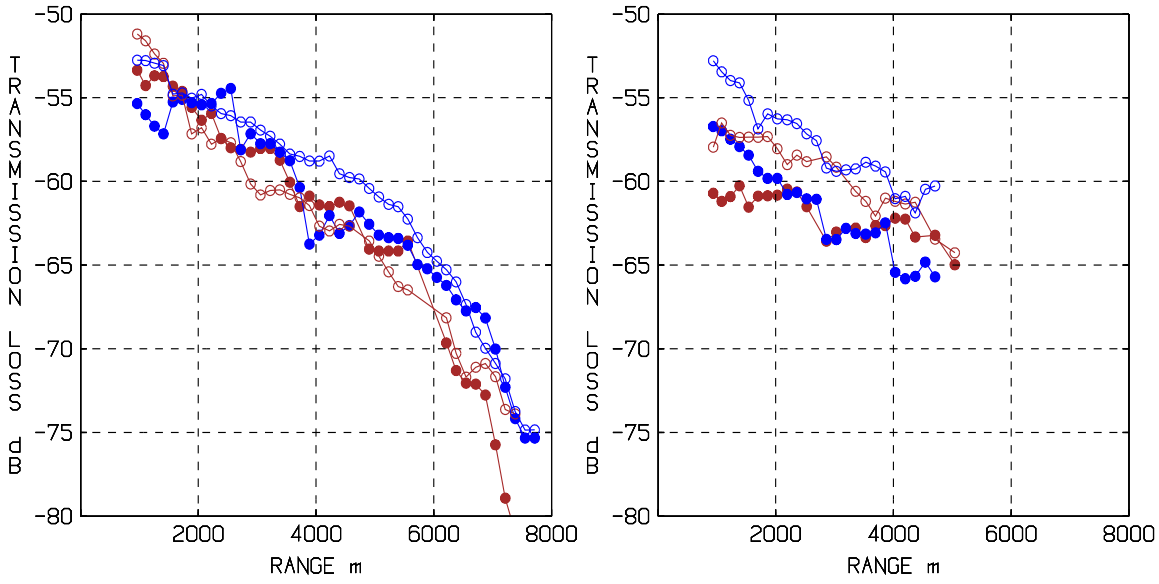

(c) 70 Hz, Fitness = 2.10 dB

(d) 120 Hz, Fitness = 3.46 dB

Figure 7.3: Result of inversion 18:4. Data (filled circles) and model (circles) for receiver depths 20 m (brown) and 60 m (blue).

7.2 Range-dependent fluid seabed: Inversion 18:3

See Tab. 5.1 for the search-intervals of the geoacoustic parameters. The resulting medium is shown in Figs. 7.5 and 7.4. The fitness values for the inversion data set and the control data sets are shown in Tab. 7.2, and Fig. 7.6 shows the agreement between the model and the inversion data curves.

We notice that the removal of the shear parameters eliminated a considerable loss-mechanism of the model. This is particularly pronounced in Fig. 7.5: the model tries to compensate for the shear wave-induced losses by choosing the lowest possible velocity (1550 m/s) of the sediment, the highest possible attenuation (1.3 dB/λ), and the largest possible sediment thickness (40 m) along the whole track. Nevertheless, the fitness values of the model curves are very poor, cfr. Fig. 7.6.

	Fitness [dB]		
Frequency [Hz]	Inversion data set	Control data set 1	Control data set 2
30	4.09	3.76	3.69
45	4.42	5.14	3.49
70	4.03	5.03	4.12
120	3.90	4.74	4.86
All 4 frequencies	4.14	4.76	4.00

Table 7.2: Inversion case 18:3. Fitness values for the inversion data set (receiver depths 20 and 60 m), control data set 1 (receiver depths 10, 50 and 70 m) and control data set 2 (receiver depth 30 m, maybe contaminated by noise, cfr. Sec. 6.6.). Cfr. Tab. 7.1.

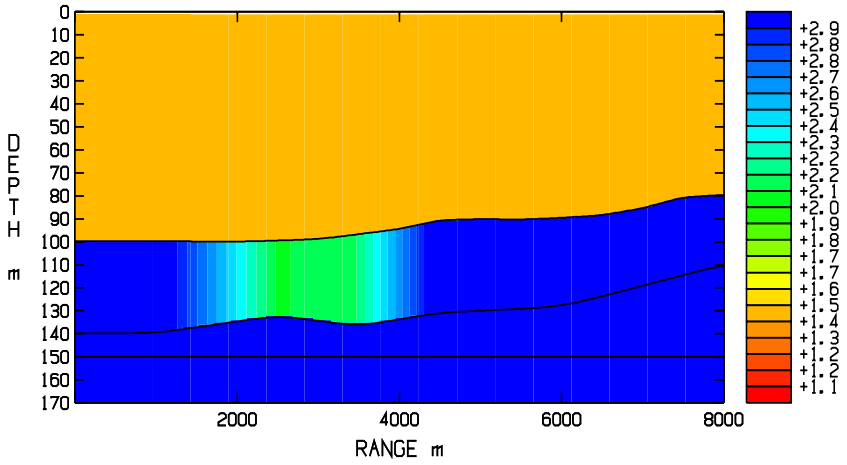

(a) The acoustic impedance (10^6 kg/m^{2}s)

Figure 7.4: The acoustic impedance obtained from inversion 18:3.

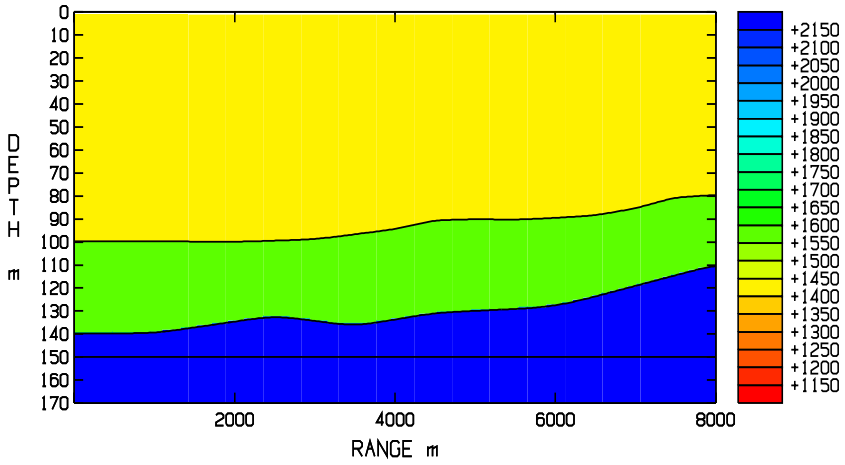

(a) P-velocity (m/s)

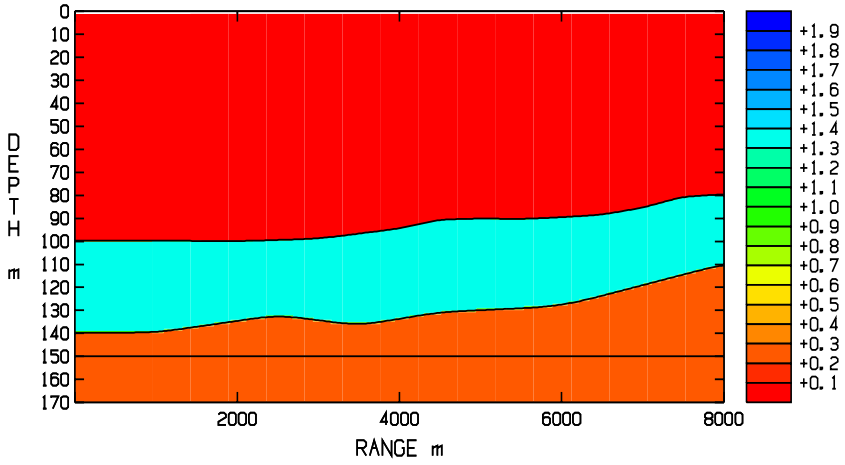

(b) P-attenuation (dB/λ)

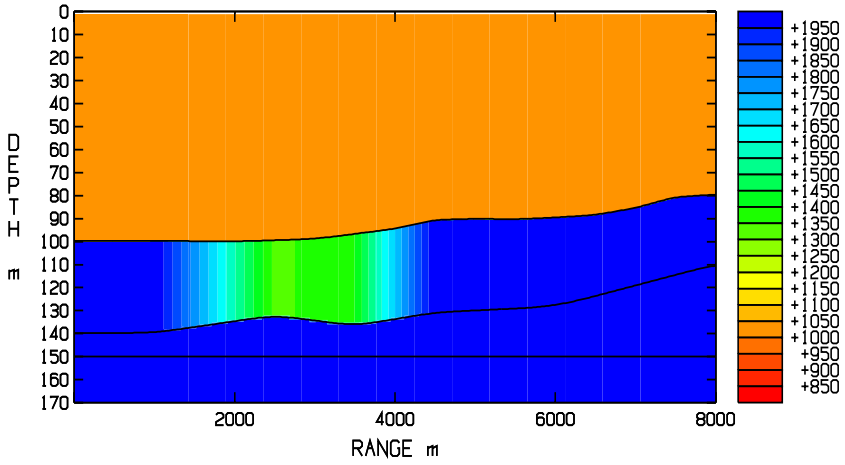

(c) Density (kg/m^3)

Figure 7.5: Media parameters obtained from inversion 18:3.

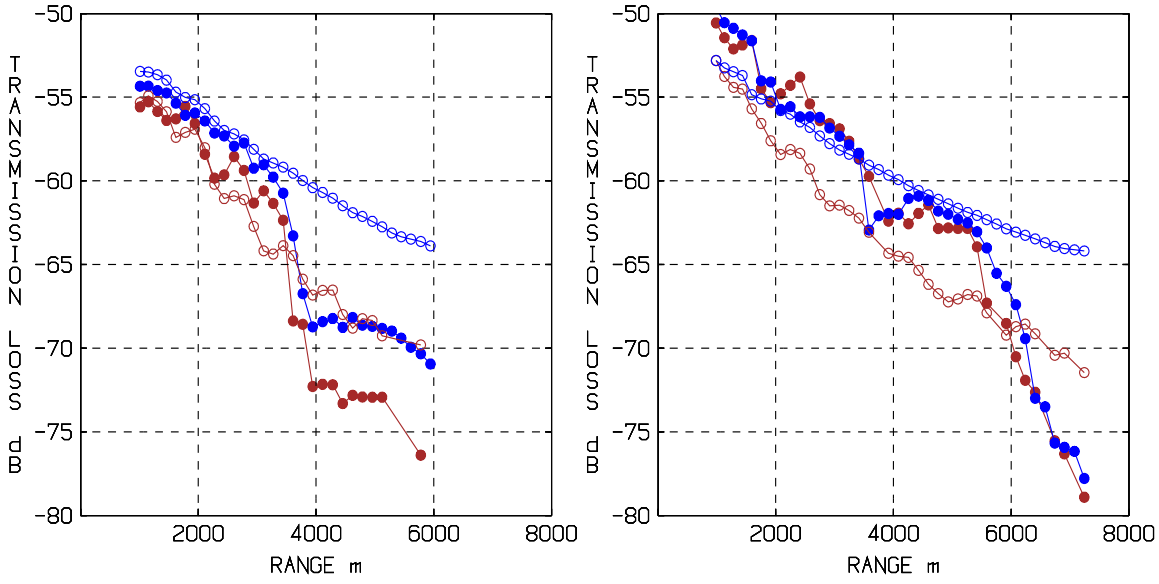

(a) 30 Hz, Fitness = 4.09 dB

(b) 45 Hz, Fitness = 4.42 dB

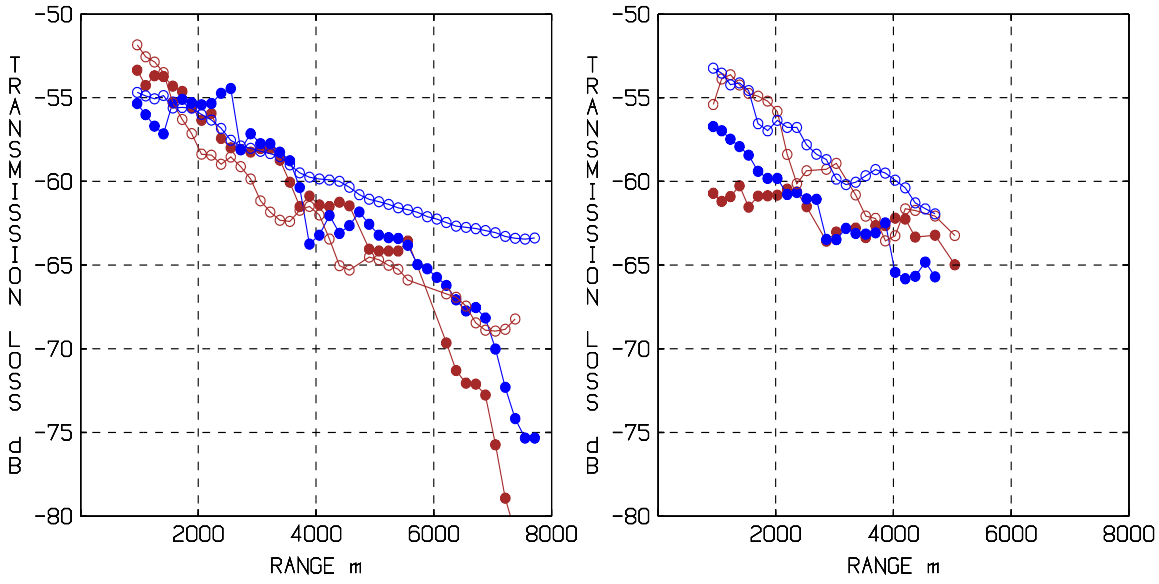

(c) 70 Hz, Fitness = 4.03 dB

(d) 120 Hz, Fitness = 3.90 dB

Figure 7.6: Result of inversion 18:3. Data (filled circles) and model (circles) for receiver depths 20 m (brown) and 60 m (blue).

7.3 Range-dependent fluid seabed with extended search space: Inversion 18:2

Since the GA tried to exceed the borders of the search space in the poor-result fluid inversion 18:3 above, we extended the limits of the search intervals for the sound velocity and attenuation in the present inversion, cfr. Tab. 5.1. The results of the inversion are shown in Figs. 7.8, 7.7 and 7.9. The fitness values for the inversion data set and the control data sets are shown in Tab. 7.3.

We notice that the thickness of the sediment varies between 10 and 30 m which agrees quite well with the expected values (5-20 m). The attenuation is largest in the middle of the track. The sound velocity is very low at the beginning of the track, increases to a maximum at the thickest part of the sediment at about 3 km whereafter it decreases to a level somewhere in between these extreme values with pockets of low velocities in the top of the sediment. It should be noted that beyond 6 km, only 45 and 70 Hz data were available for the inversion.

The introduction of very low sediment velocities seems to have compensated for losses caused by shear wave excitation in the solid model. The agreement between the data and the model turned out to be very good apart from 120 Hz: as for the solid media model, this fluid model seems to adapt quite well to the decay characteristics at depth 60 m (blue curve in Fig. 7.9), but the overall level of the TL is about 2-3 dB too high in the model at this frequency and depth. The uncertainty in the result of 120 Hz is clearly illustrated when the model is run against the control data sets. A similar shakiness in the 30 Hz-result is noticed when the model is run against control data set 1. This could be an effect of a drawback of PE-approximations in general: At very low frequencies the basic assumption of the PE-approximation, i.e. that the main propagation direction is almost horizontal, might not be fulfilled. This is further discussed in Sec. 7.5 below.

	Fitness [dB]		
Frequency [Hz]	Inversion data set	Control data set 1	Control data set 2
30	2.00	3.61	2.22
45	1.64	2.77	2.41
70	1.85	3.10	2.17
120	2.58	4.47	4.32
All 4 frequencies	1.98	3.40	2.77

Table 7.3: Inversion case 18:2. Fitness values for the inversion data set (receiver depths 20 and 60 m), control data set 1 (receiver depths 10, 50 and 70 m) and control data set 2 (receiver depth 30 m, maybe contaminated by noise, cfr. Sec. 6.6.).

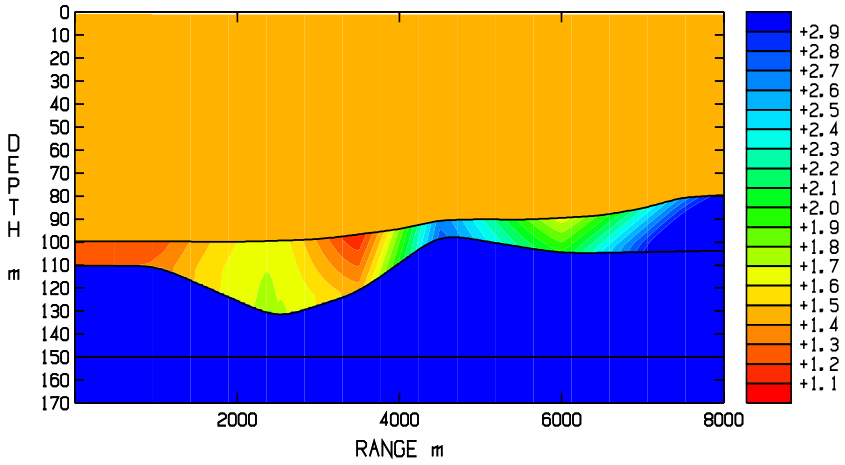

(a) The acoustic impedance (10^6 kg/m^{2}s)

Figure 7.7: The acoustic impedance obtained from inversion 18:2.

7.3.1 Effect of range-dependent sound velocity profile

The variation of the sound velocity with range and depth was continuously registered along the tracks during the experiment. However, the CTD-chain covered only the upper 50 m of the water volume, cfr. Fig. 2.2. One of the profiles in Fig. 2.3 (the one registered closest in time to the run) was used for extending these data below 50 m. The result is shown in Fig. 7.10. The fitness values for the inversion data set and the control data sets when the model obtained from inversion 18:2 was run with this very slowly varying range-dependent velocity profile of the water are shown in Tab. 7.4. As expected, the range-dependent profile has almost no effect on the wave propagation, cfr. Tab. 7.3.

Frequency [Hz]	Fitness [dB]		
	Inversion data set	Control data set 1	Control data set 2
30	2.03	3.65	2.25
45	1.61	2.76	2.37
70	1.88	3.11	2.25
120	2.59	4.30	4.52
All 4 frequencies	1.99	3.38	2.84

Table 7.4: Medium obtained from inversion 18:2. Model run with a range-dependent sound velocity profile in the water. Fitness values for the inversion data set (receiver depths 20 and 60 m), control data set 1 (receiver depths 10, 50 and 70 m) and control data set 2 (receiver depth 30 m, maybe contaminated by noise, cfr. Sec. 6.6.). Cfr. the results when the model was run with the range-independent profile of the inversion, Tab. 7.3

7.3.2 Effect of source depth variation

The variation of the source depth along the tracks was about ±2 m, cfr. Sec. 5.9. Figure 7.11 shows the variation of the fitness value as the source depth is varied in an interval ±3 m around the average value 37.0 m used in the inversions. As expected, errors due to varying source depth along the tracks are of minor importance. The variation is within some tenths dB apart from 120 Hz where the variation could be as large as 1 dB, but this is still within the margins of error discussed at the end of Sec. 5. The larger sensitivity at 120 Hz could be an effect of the strange behaviour of these data (cfr. Sec. 7.1) which none of the inversion models succeeded to match well.

7.3.3 Effect of uncertainty in the source-receiver separation and sparse data sampling

The uncertainty in the source-receiver separation was about ±100 m, cfr. Sec. 5.9. Figure 7.12 shows the variation of the fitness value as the output range grid in JEPE-S is translated ±100 m around the range grid used in the inversion. The variation is roughly within 1 dB and is probably an effect of the sparse data sampling as well as the difference in source-receiver separation, cfr. Fig. 7.13. The mean l_2-norm of the difference between the solutions computed on the dense range-grids with stepsize 1 m translated 75 m with respect to each other is 0.53 dB, which is well in accordance with the estimation in Sec. 5.9, while for the sparse data grid used in the inversion the corresponding difference is 1.34 dB. The sparse-grid solutions differ the most at small ranges. Uncertainties due to sparse data sampling was discussed in Sec. 5.10.

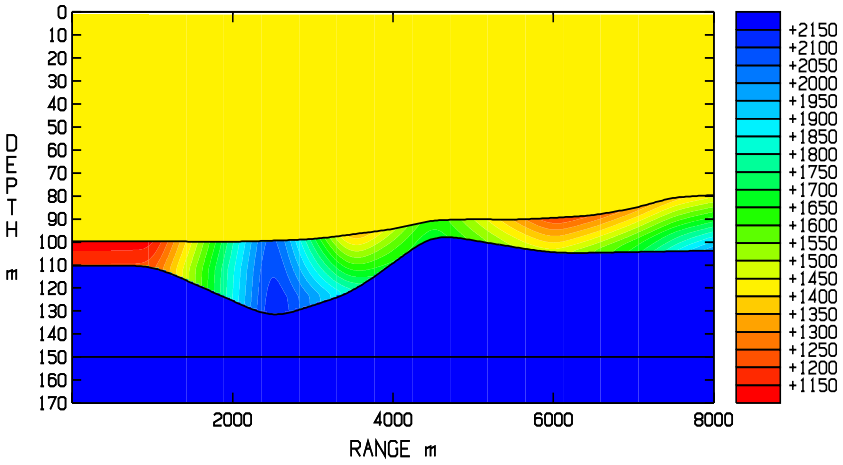

(a) P-velocity (m/s)

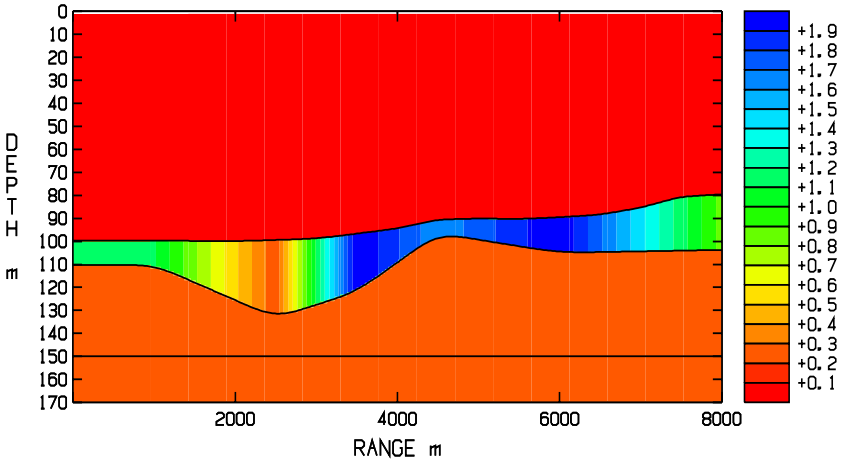

(b) P-attenuation (dB/λ)

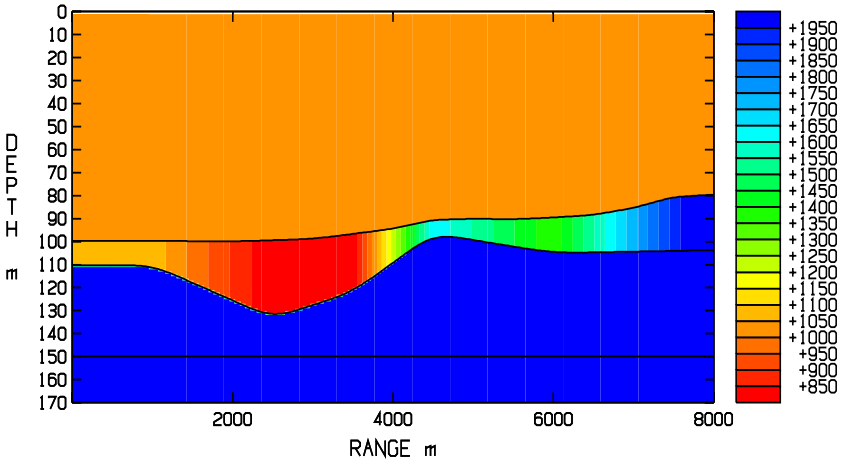

(c) Density (kg/m^3)

Figure 7.8: Media parameters obtained from inversion 18:2.

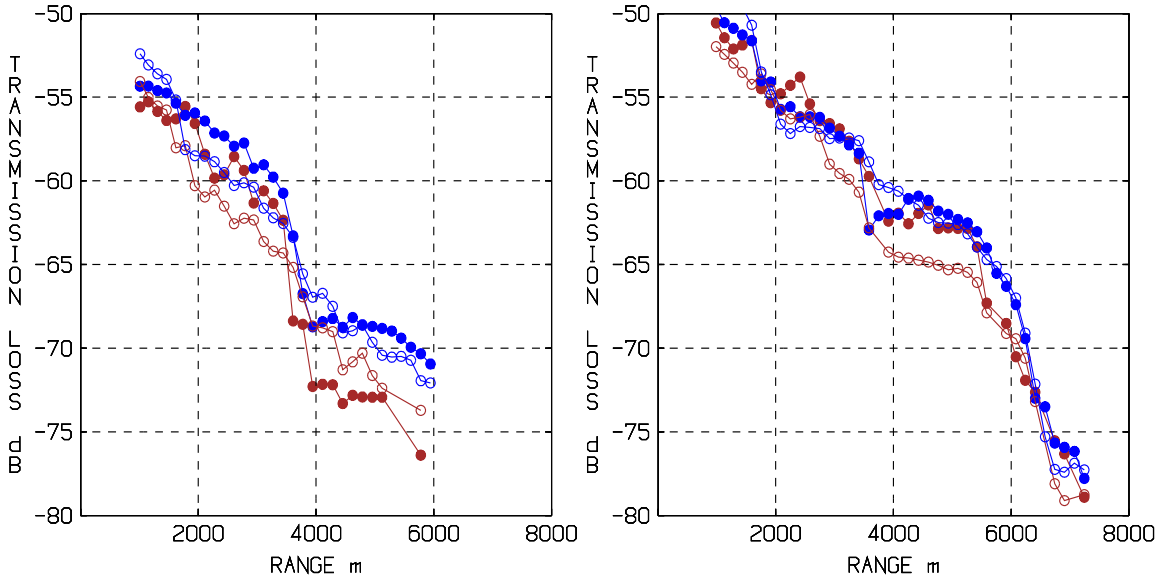

(a) 30 Hz, Fitness = 2.00 dB

(b) 45 Hz, Fitness = 1.64 dB

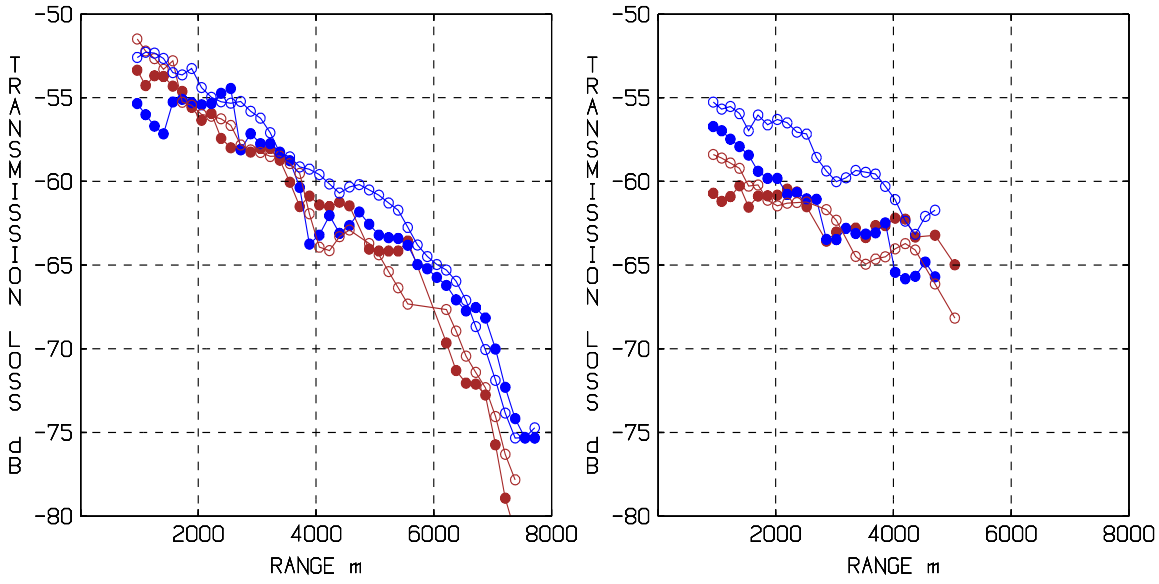

(c) 70 Hz, Fitness = 1.85 dB

(d) 120 Hz, Fitness = 2.58 dB

Figure 7.9: Result of inversion 18:2. Data (filled circles) and model (circles) for receiver depths 20 m (brown) and 60 m (blue).

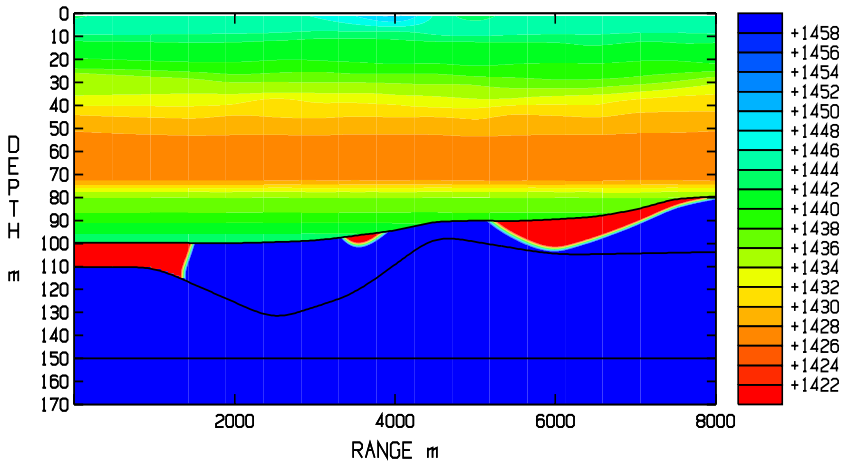

(a) Sound velocity (m/s)

Figure 7.10: Range-dependent sound velocity profile of the water. The variation with range in the upper 50 m is very small, below 50 m the velocity is constant w.r.t. range.

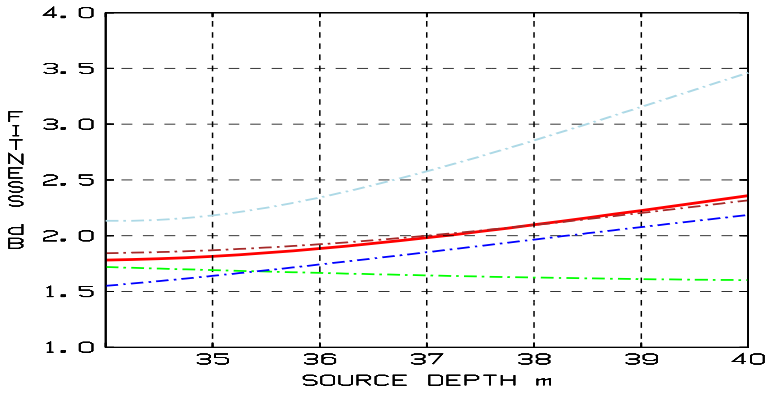

(a) Fitness as function of source depth.

Figure 7.11: Variation of the fitness value as the source depth is varied around the average depth used in the inversion. The model is run on the media obtained from inversion 18:2. Fitness based on all four frequencies (red line), on data for 30 Hz (brown), 45 Hz (green), 70 Hz (blue) and 120 Hz (light blue).

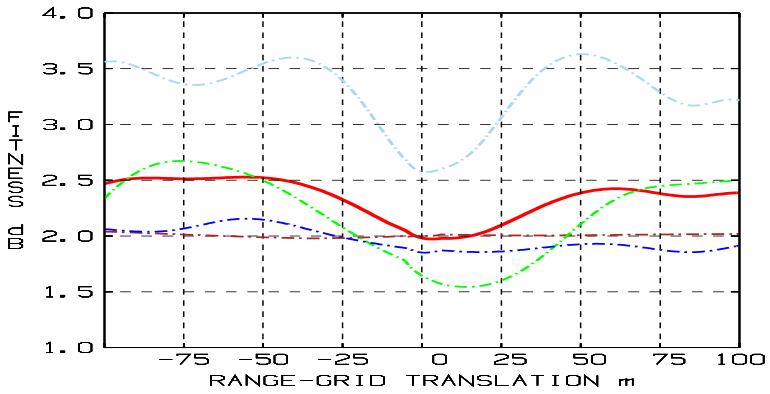

Figure 7.12: Variation of the fitness value as the output range-grid is translated ±100 m from that used in inversion 18:2. Fitness based on all four frequencies (red line), on data for 30 Hz (brown), 45 Hz (green), 70 Hz (blue) and 120 Hz (light blue).

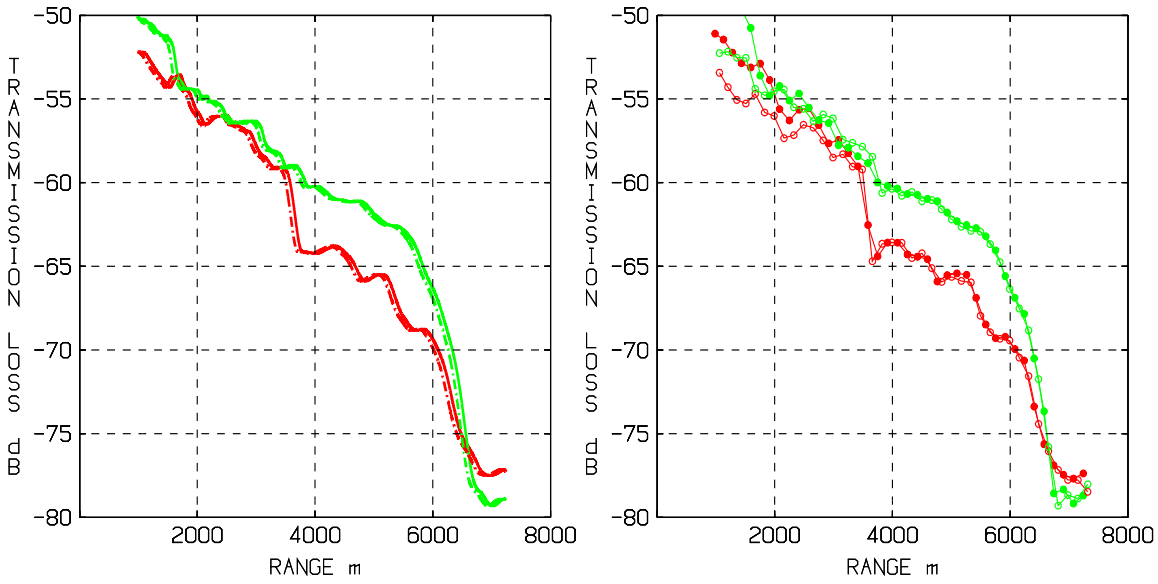

(a) Stepsize 1 m in output range grid. Original grid (continuous lines) and translated 75 m to the right (dashed lines). The mean l_2-norm of the difference between the solutions is 0.53.

(b) Stepsize about 150-200 m in output range grid. Solution computed at the gridpoints used in the inversion (filled circles), and at a grid translated 75 m to the right (circles). The mean l_2-norm of the difference between the solutions is 1.34.

Figure 7.13: 45 Hz solution computed for media model obtained from inversion 18:2. Receiver depths 20 m (red) and 60 m (green).

7.4 An alternative fitness function: Inversion 18:2B

When the absolute level of the data is uncertain due to uncalibrated receivers and/or transmitters, or the level of the computed TL is doubtful due to drawbacks of the model like for example the difficulty for a PE-model to handle very low frequencies at shallow depths and thin sediments, can a media model still be found which predicts the transmission loss sufficiently accurate?

In this subsection we compare the result of inversion 18:2 in Sec. 7.3 with that obtained using the alternative fitness function described in Sec. 5.5. This alternative fitness function is independent of the absolute level of the data and thus the inversion uses information of the relative decay rates in the data only. The results are found in Figs. 7.15, 7.14, 7.16, and Tabs. 7.5, 7.6.

Except at the beginning of the track, the media model obtained with this alternative objective function is largely consistent with that of inversion 18:2. It mainly differs at about 4-5 km, and the reason seems to be that in this case the model succeeds to adapt better to the drop in the data between 3 and 5 km. When relieved from the task of adapt to the absolute level of the data, the model can focus entirely on the adaptation to the local variations of the TL-curves. This example indicates that the method of matching only the relative decay of the data presumably works well.

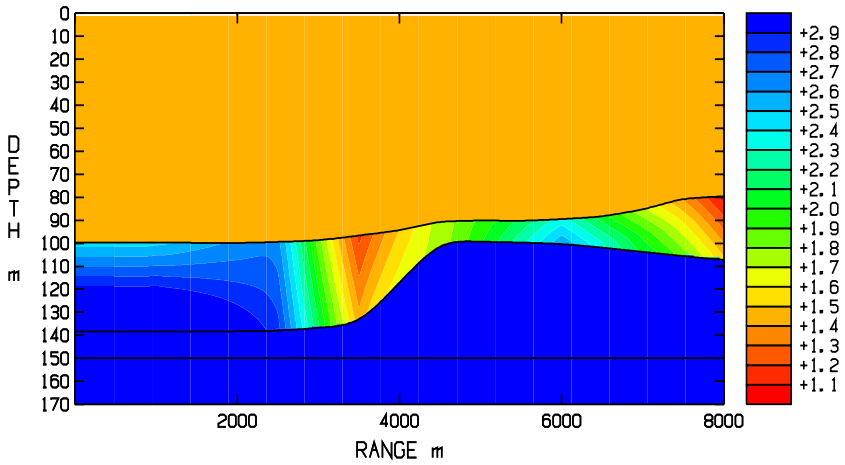

(a) The acoustic impedance (10^6 kg/m^{2}s)

Figure 7.14: The acoustic impedance obtained from inversion 18:2B, cfr. Fig. 7.7.

Frequency [Hz]	Fitness [dB]		
	Inversion data set	Control data set 1	Control data set 2
30	1.69	2.07	1.78
45	1.38	2.30	0.92
70	1.32	2.50	2.09
120	1.64	2.96	2.91
All 4 frequencies	1.49	2.44	1.95

Table 7.5: Inversion case 18:2B. Fitness values computed by the alternative fitness function for the inversion data set (receiver depths 20 and 60 m), control data set 1 (receiver depths 10, 50 and 70 m) and control data set 2 (receiver depth 30 m, maybe contaminated by noise, cfr. Sec. 6.6.). Cfr. Tabs. 7.3 and 7.6

Frequency [Hz]	Fitness [dB]		
	Inversion data set	Control data set 1	Control data set 2
30	4.43	3.96	4.08
45	1.44	2.39	1.10
70	2.04	2.58	2.58
120	4.67	5.73	5.73
All 4 frequencies	3.20	3.59	3.49

Table 7.6: Inversion case 18:2B. Fitness values computed by the original fitness function for the inversion data set (receiver depths 20 and 60 m), control data set 1 (receiver depths 10, 50 and 70 m) and control data set 2 (receiver depth 30 m, maybe contaminated by noise, cfr. Sec. 6.6.). Media model the same as in Tab. 7.5. Cfr. Tab. 7.3

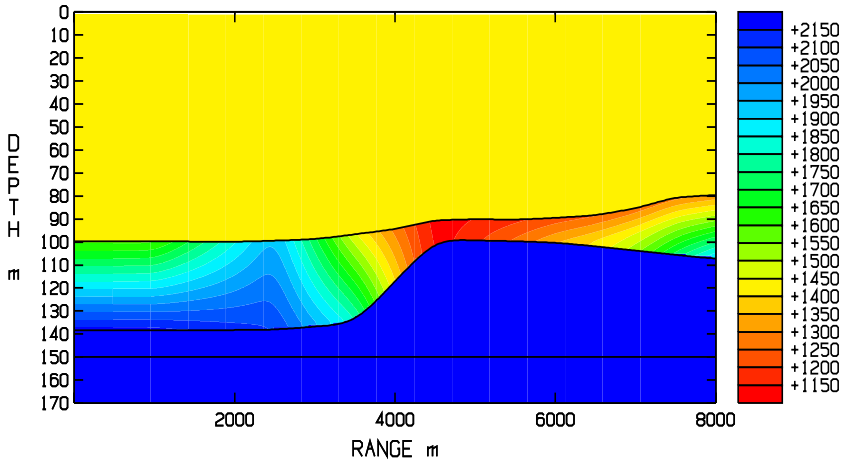

(a) P-velocity (m/s)

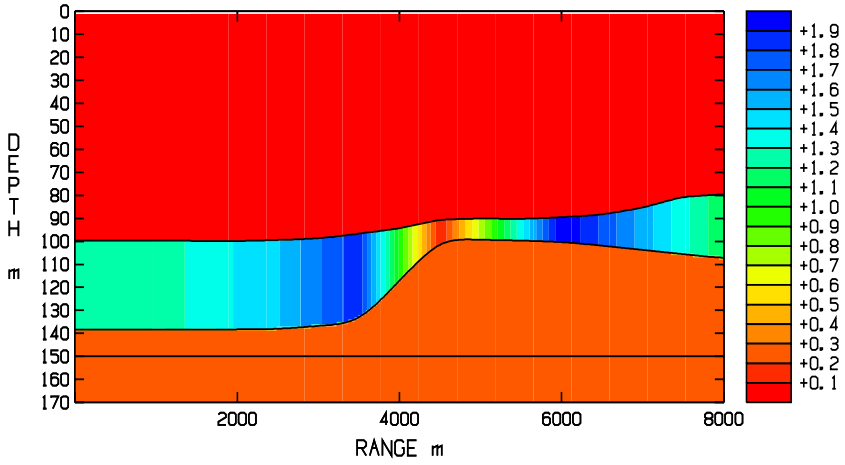

(b) P-attenuation (dB/λ)

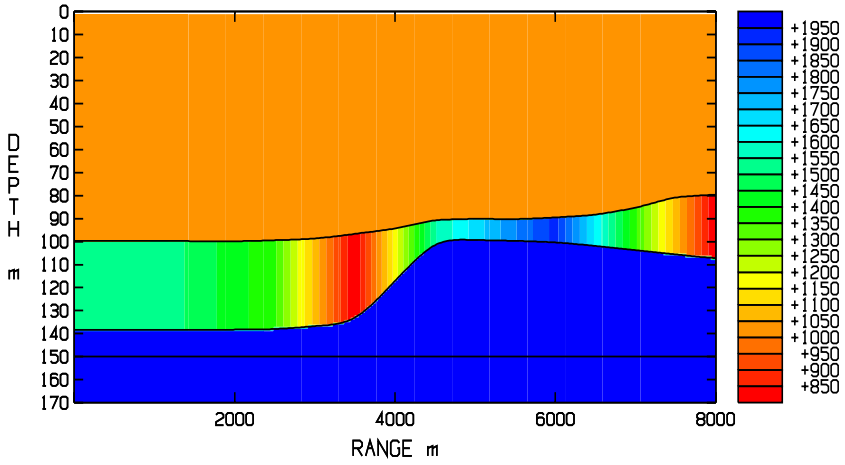

(c) Density (kg/m^3)

Figure 7.15: Media parameters obtained from inversion 18:2B, cfr. Fig. 7.8

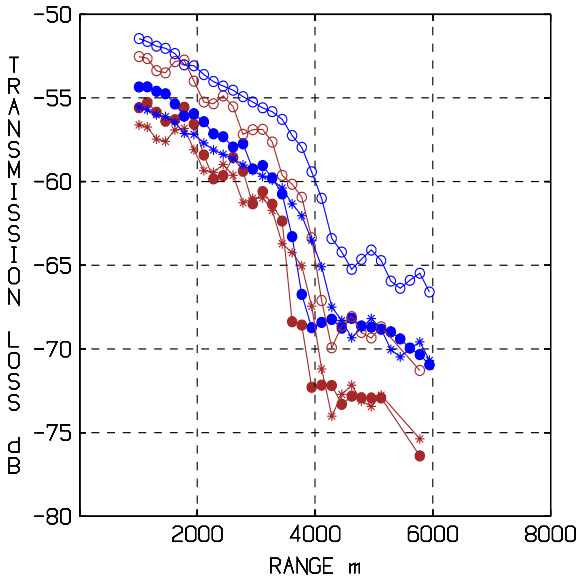

(a) 30 Hz, Fitness = 1.69 (4.43) dB. Within parenthesis the fitness value for the model solution (circles) which is not vertically translated.

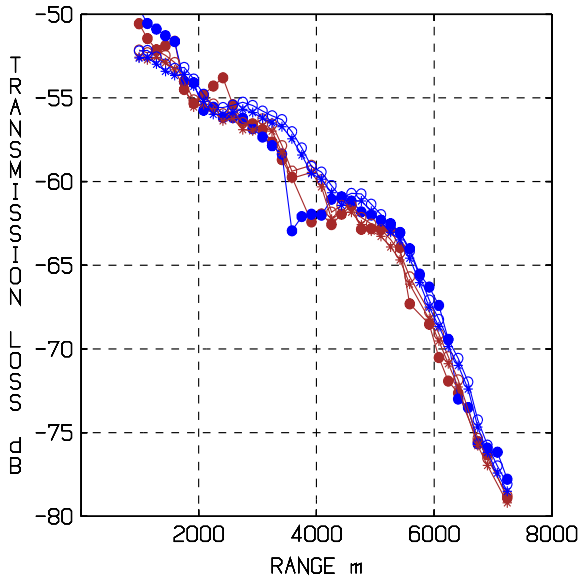

(b) 45 Hz, Fitness = 1.38 (1.44) dB. Within parenthesis the fitness value for the model solution (circles) which is not vertically translated.

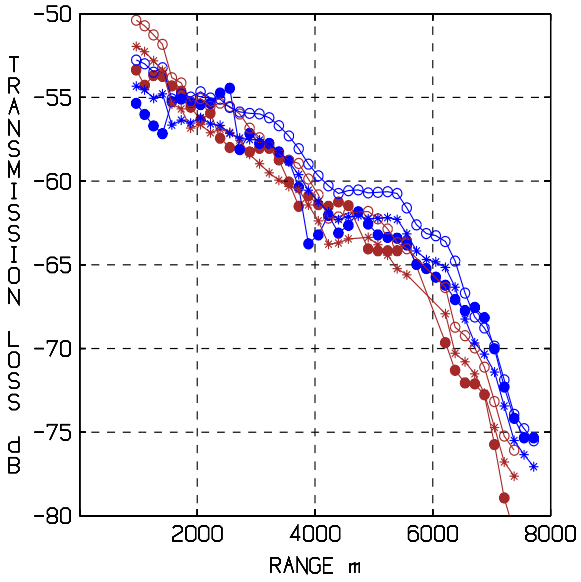

(c) 70 Hz, Fitness = 1.32 (2.04) dB. Within parenthesis the fitness value for the model solution (circles) which is not vertically translated.

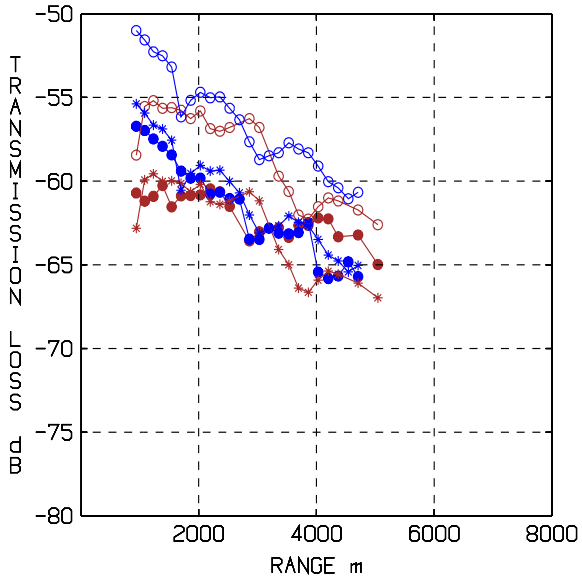

(d) 120 Hz, Fitness = 1.64 (4.67) dB. Within parenthesis the fitness value for the model solution (circles) which is not vertically translated.

Figure 7.16: Result of inversion 18:2B. Data (filled circles), model (circles) and vertically translated model values used in the evaluation of the fitness function (asterisks) for receiver depths 20 m (brown) and 60 m (blue), cfr. Fig. 7.9

7.5 Range-independent fluid seabed: Inversion 18:1

See Tab. 5.1 for the search-intervals of the geoacoustic parameters. The result of the inversion is shown in Tab. 7.7 and Fig. 7.17. The fitness values for the inversion data set and the control data sets are shown in Tab. 7.8.

The agreement between model and data is surprisingly good for this simple model, with a mismatch of about 3 dB for the three lowest frequencies. The 120 Hz data are poorer, but as already noticed, none of the inversion models, regardless of the degree of complexity, succeeded to match this frequency.

Water Depth	c_p^{top} [m/s]	c_p^{bot} [m/s]	β_p [dB/λ]	ρ [kg/m^3]	Sediment thickness [m]
90.8	1327	1327	0.35	2107	27.7

Table 7.7: Media parameters obtained from inversion 18:1 with a range-independent geometry and fluid seabed. β_p denotes the attenuation, ρ the density, and c_p^{top} and c_p^{bot} the sound velocity at the top and the bottom respectively of the sediment.

	Fitness [dB]		
Frequency [Hz]	Inversion data set	Control data set 1	Control data set 2
30	3.03	3.14	3.39
45	1.79	3.12	4.46
70	3.17	3.78	3.89
120	3.04	4.83	4.07
All 4 frequencies	2.78	3.68	4.00

Table 7.8: Inversion case 18:1. Fitness values for the inversion data set (receiver depths 20 and 60 m), control data set 1 (receiver depths 10, 50 and 70 m) and control data set 2 (receiver depth 30 m, maybe contaminated by noise, cfr. Sec. 6.6.).

The inversion resulted in a water depth which is roughly equal to the average depth along the track, cfr. Fig. 2.2. We also notice the low velocity of the sediment, well below both the sound velocity of the water and the velocity expected for the type of sediment at this test site. This raises questions about the reliability of the PE-model being used. As already pointed out in Sec. 4 above, a PE-model relies on the fact that modes propagating with high angles are lost due to penetration into the seabed at an early stage, leaving only modes within a narrow angle relative to the horizontal to propagate over long ranges. If the velocity of the seabed is lower than that of the water, then it would be natural to expect that all modes will penetrate into the seabed and therefore have comparable decay rates. If therefore modes with high propagation angles are sufficiently strongly excited in the source field, then their effect on the propagating wavefield might not be negligible, thus violating the basic assumption of the PE-approximation. To find out if this is the case for the media model obtained from this inversion, we compared the solution computed by JEPE-S with that computed by the full field code XFEM [8], see Fig. 7.18.

Obviously, the low-velocity seabed did pose no problem for the PE-model. The agreement between the two models is very good for 45, 70 and 120 Hz. The disagreement in the 30 Hz-case is due to a drawback of PE-approximations in general and not to the low-velocity seabed in particular: At low frequencies, shallow depths and thin sediments above bedrock the number of propagating modes is small and modes with large elevation angle and small decay rate may exist. This implies that modes outside the angle-interval supported by the PE can give a considerable contribution to the wavefield. In our case this is the case for 30 Hz, but not for the higher frequencies. By confining the source in XFEM to the mode-angles supported by JEPE-S, then also the 30 Hz-curves did agree well. Therefore, the 30 Hz-results of the inversions should be interpreted with some care. The reason for why not all modes, regardless of propagation angle, penetrate into the seabed and get trapped there is most probably due to the high value of the density (2107 kg/m^3) which implies a large impedance contrast between the water and the seabed in spite of the low velocity of the bottom.

7.5.1 Sensitivity analysis

A sensitivity analysis gives an idea about how much information about the seabed that might be extracted from the observed data. The medium obtained from inversion 18:1 above was chosen to form the base model for the sensitivity analysis. Each parameter, one at a time, was then changed with a small amount whereupon the model was run on the inversion data set and the fitness value was computed. The results are shown in Fig. 7.19.

The GA seems to have managed to locate the global minimum of the objective function (red lines). However, there are discrepancies in the behaviour between the different frequencies. The lowest frequency (30 Hz, brown curves) seems to differ the most from the other frequencies. This could be due to the large wavelengths which makes it more difficult to recognize the details of the media. It could also be an effect of the difficulty for the PE-model to handle very low frequencies, cfr. Fig. 7.18. We also notice the similar behaviour of the fitness value as function of the sound velocity wheter the density is constant or is varied in order to make the impedance attain the optimum value of the inversion. This is probably due to the large value of the density in both cases, i.e. the impedance contrast is large in both these cases. According to the 70 and 120 Hz curves (blue and light blue) a candidate for the value of the sediment velocity could also be 1450 m/s. The most unique global minimum of the fitness function is obtained for the attenuation, it is unambiguously the same for all four frequencies. This parameter is also the one which is most important. The thickness and the sound velocity of the sediment are also important parameters, while the water depth seems to be of minor importance in this model.

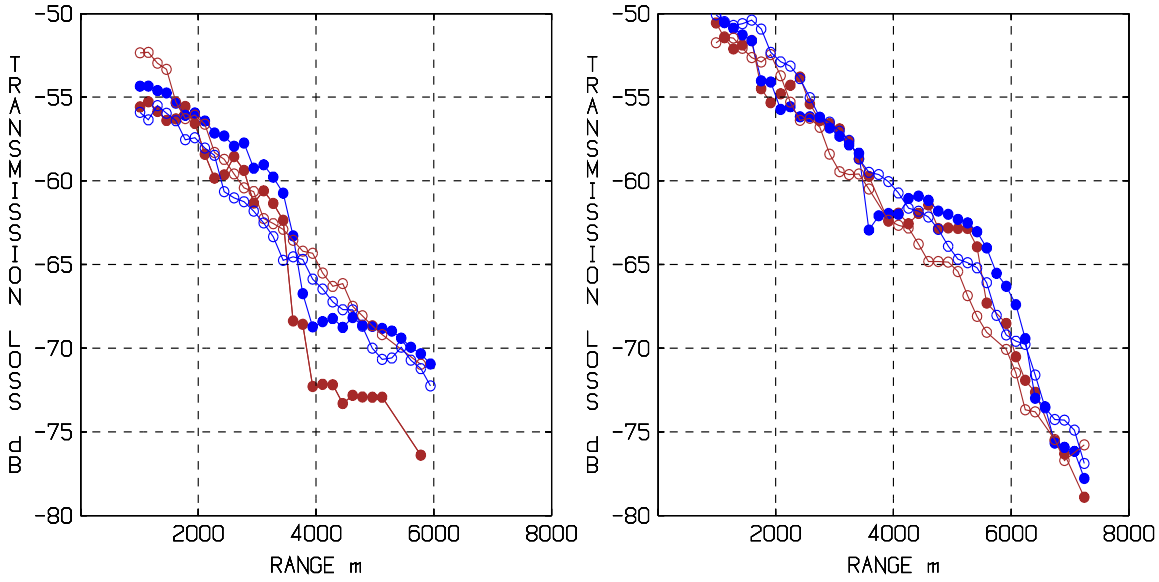

(a) 30 Hz, Fitness = 3.03 dB

(b) 45 Hz, Fitness = 1.79 dB

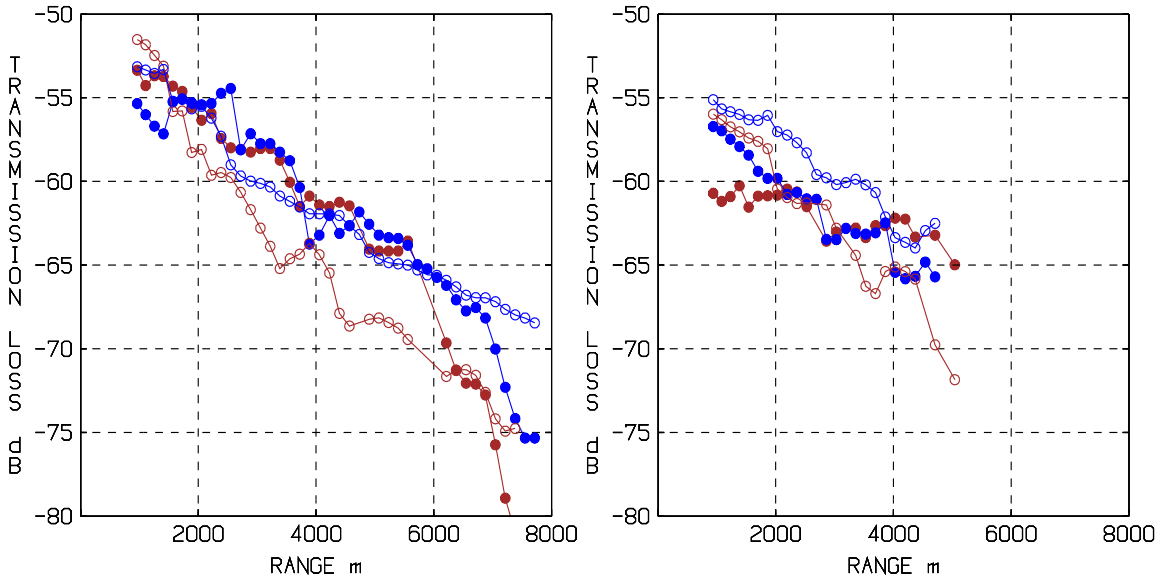

(c) 70 Hz, Fitness = 3.17 dB

(d) 120 Hz, Fitness = 3.04 dB

Figure 7.17: Result of inversion 18:1. Data (filled circles) and model (circles) for receiver depths 20 m (brown) and 60 m (blue).

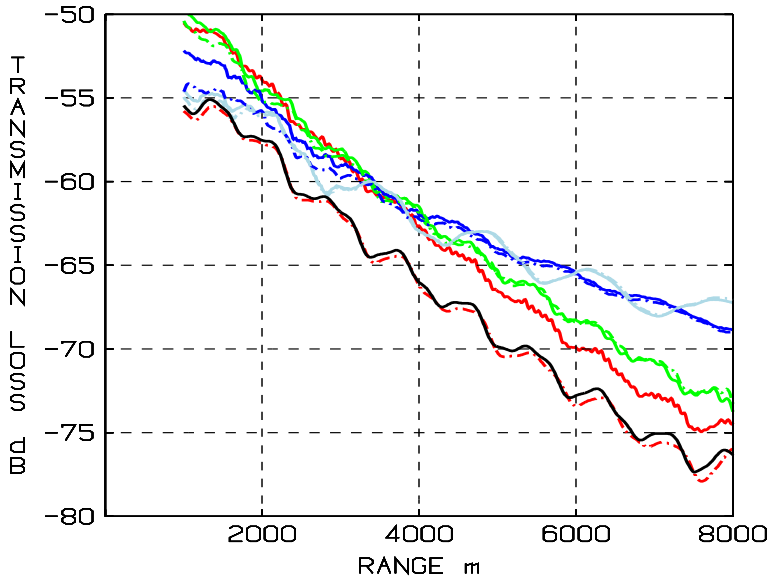

Figure 7.18: Comparison between wavefields computed by XFEM (continuos lines) and JEPE-S (dashed lines) on receiver depth 60 m for frequencies 30 Hz (red), 45 Hz (green), 70 Hz (blue) and 120 Hz (light blue) for media parameters obtained from inversion 18:1. The agreement between the two models is good except for 30 Hz. The black line shows the 30 Hz solution computed by XFEM with a source confined to the first three propagating modes within the angle interval supported by JEPE-S. This solution agrees well with that computed by JEPE-S.

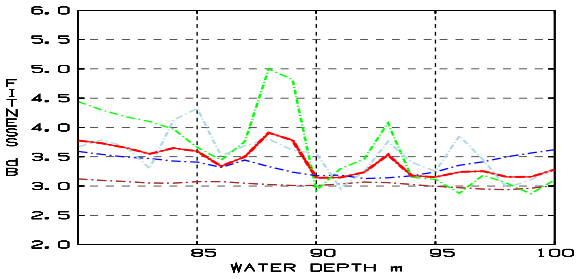

(a) Fitness as function of water depth.

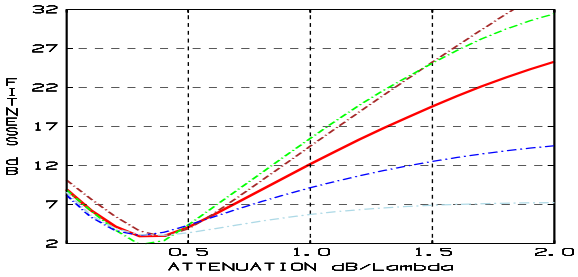

(b) Fitness as function of attenuation.

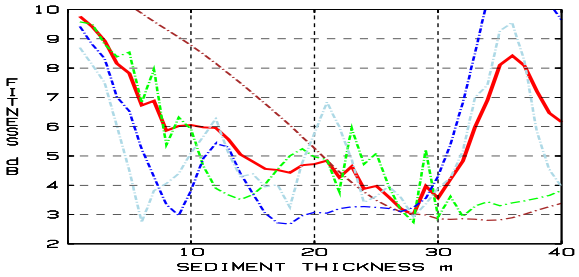

(c) Fitness as function of sediment thickness.

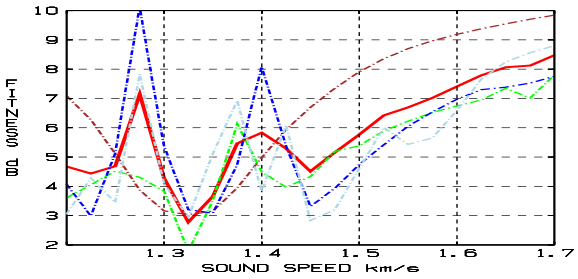

(d) Fitness as function of sound velocity.

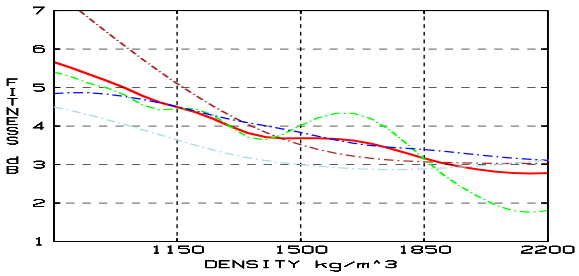

(e) Fitness as function of density.

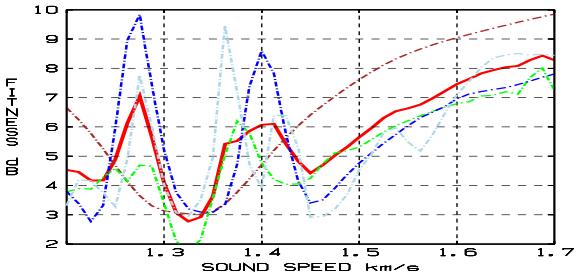

(f) Fitness as function of sound velocity when the impedance is constant and equals the optimum value of the inversion.

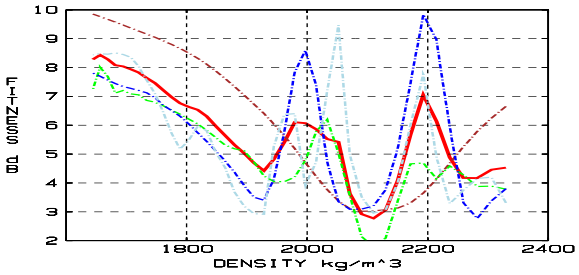

(g) Fitness as function of density when the impedance is constant and equals the optimum value of the inversion.

Figure 7.19: Variation of the fitness value as the parameters of inversion 18:1 are varied. Fitness based on all four frequencies (red line), on data for 30 Hz (brown), 45 Hz (green), 70 Hz (blue) and 120 Hz (light blue).

8 Inversion results: Run 19

As in Sec. 7 above, we begin with the result for the most complex model, that is, the range-dependent solid seabed model (Sec. 8.1), and then gradually reduce the complexity down to a horizontally stratified fluid seabed model (Sec. 8.4). Sensitivity analysis is confined to the least complex model.

The solid seabed model 19:4 in Tab. 6.1 succeeds to match the three lowest frequencies very well apart from small-scale details in the interference patterns of the 45 and 70 Hz data, cfr. Fig 8.2 (Sec. 8.1). The fluid seabed model 19:3, obtained with the same realistic search intervals as 19:4, was less successful, especially at 30 and 70 Hz, cfr. Fig. 8.6 (Sec. 8.2). Both models fail completely to match the 120 Hz data.

The fluid seabed model with unrealistic search intervals, 19:2, however fits excellently to the data at all four frequencies, cfr. Fig. 8.9 (Sec. 8.3).

Finally, the inversion with the simplest model, 19:1, resulted in a range-independent model with a very hard seabed, and water depth 90 m (which is below the minimum depth along the track). A sensitivity analysis shows that the water depth would be reduced further if the search interval had been wider, this in order to compensate for the small decay rate of the data in the second half of the track, cfr. Fig. 8.11 (Sec. 8.4). Of course, a range-independent model cannot reproduce the range-dependent characteristics in the TL curves.

8.1 Range-dependent solid seabed: Inversion 19:4

See Tab. 5.1 for the search-intervals of the geoacoustic parameters. The resulting medium is shown in Figs. 8.1 and 8.3. The fitness values for the inversion data set and the control data sets are shown in Tab. 8.1, and Fig. 8.2 shows the observed and the modelled TL as function of range.

	Fitness [dB]		
Frequency [Hz]	Inversion data set	Control data set 1	Control data set 2
30	1.15	1.65	1.09
45	1.58	2.70	1.93
70	2.64	2.39	4.35
120	4.70	4.84	3.62
All 4 frequencies	2.65	2.93	2.95

Table 8.1: Inversion case 19:4. Fitness values for the inversion data set (receiver depths 20 and 60 m), control data set 1 (receiver depths 10, 50 and 70 m) and control data set 2 (receiver depth 30 m, maybe contaminated by noise, cfr. Sec. 6.6.).

The solid seabed model succeeded to match the three lowest frequencies very well, apart from small scale features of the interference patterns of the 45 and 70 Hz data,

cfr. Fig. 8.2. However, the match of the 120 Hz data is quite poor, in particular at receiver depth 60 m, as seen in Fig. 8.2 (d). The reason for this is at present not clear.

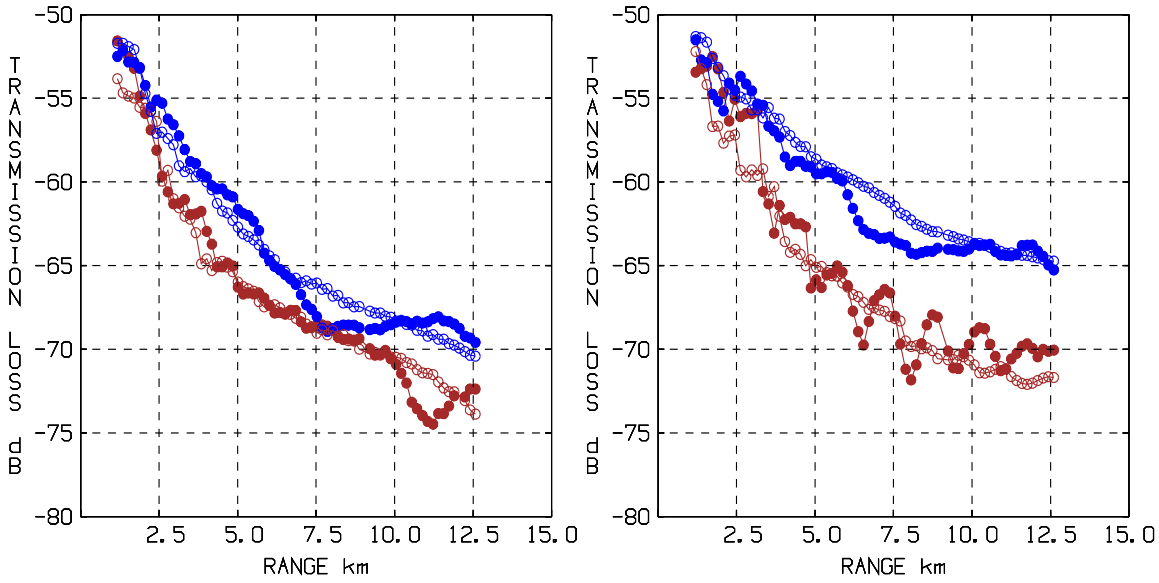

(a) 30 Hz, Fitness = 1.15 dB

(b) 45 Hz, Fitness = 1.58 dB

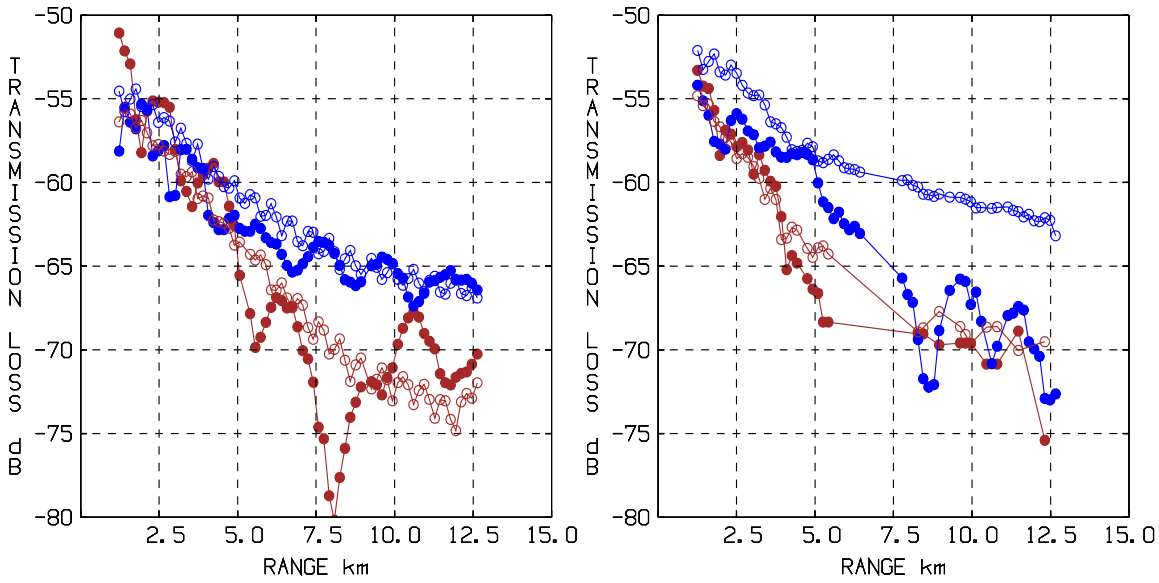

(c) 70 Hz, Fitness = 2.64 dB

(d) 120 Hz, Fitness = 4.70 dB

Figure 8.1: Result of inversion 19:4. Data (filled circles) and model (circles) for receiver depths 20 m (brown) and 60 m (blue).

We remark that, as for inversion 18:4, the solid seabed model satisfies the bulk-modulus condition for physical realizability, see Sec. 7.1 above.

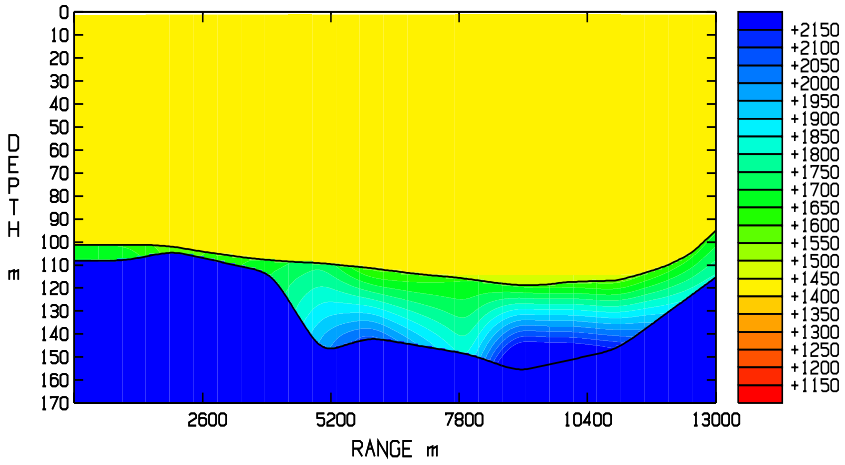

(a) P-velocity (m/s)

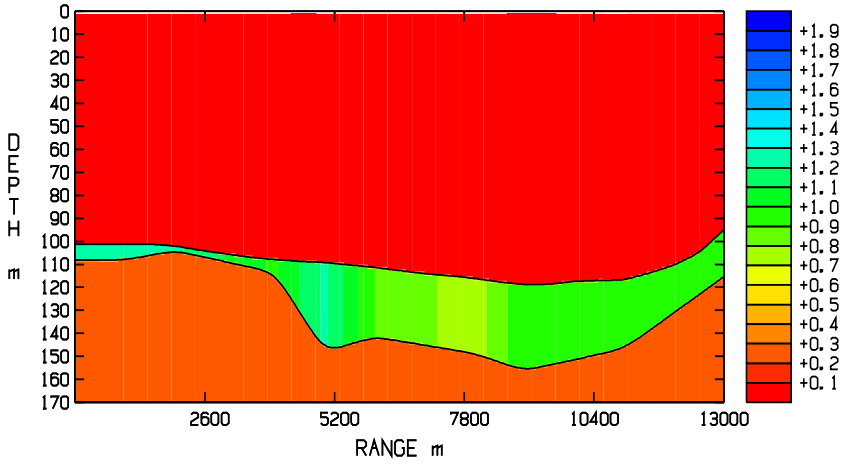

(b) P-attenuation (dB/λ)

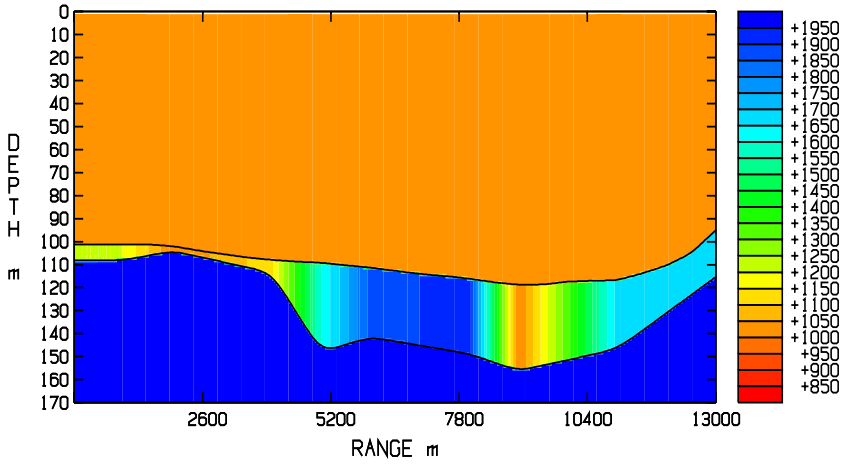

(c) Density (kg/m^3)

Figure 8.2: Media parameters obtained from inversion 19:4.

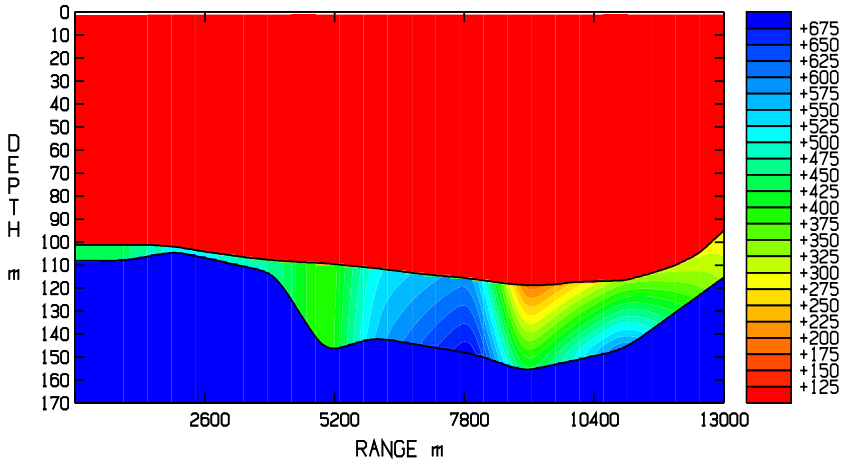

(a) S-velocity (m/s)

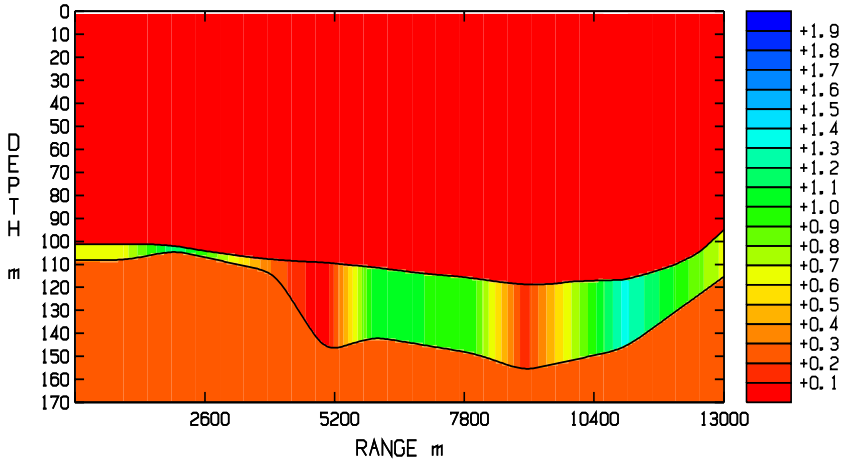

(b) S-attenuation (dB/λ)

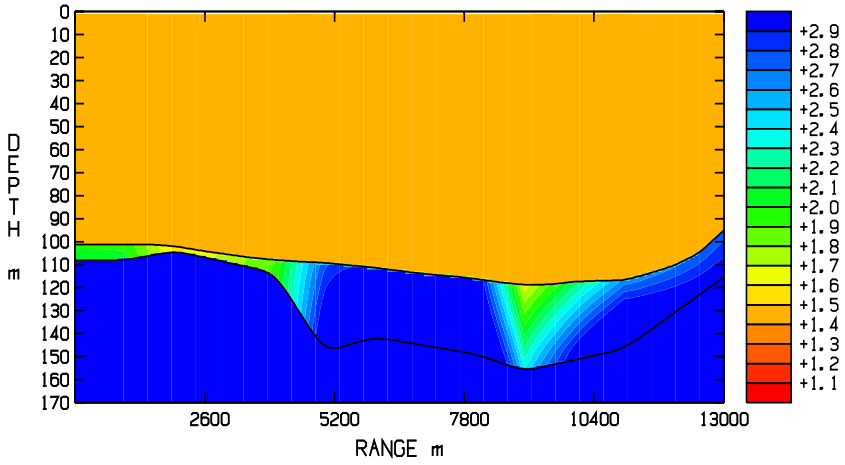

(c) The acoustic impedance (10^6 kg/m^{2}s)

Figure 8.3: Shear parameters and acoustic impedance obtained from inversion 19:4.

8.2 Range-dependent fluid seabed: Inversion 19:3

The search intervals for the fluid seabed parameters are the same as for the solid seabed case 19:4, see Tab. 5.1. The resulting medium is shown in Figs. 8.5 and 8.4. The fitness values for the inversion data set and the control data sets are shown in Tab. 8.2, and Fig. 8.6 shows the observed and the model predicted TL as function of range.

We notice that the removal of the shear parameters resulted in a deterioration in the data fitting for 30 Hz and 70 Hz, compare Figs. 8.6 and 8.2. The matching of the 120 Hz data failed as in the solid seabed case.

Notable is that the GA chose a rather thick sediment with the lowest possible velocity and highest possible attenuation along the track, that is, the same behaviour as in the corresponding fluid inversion 18:3 in Sec. 7.2 above.

Frequency [Hz]	Fitness [dB]		
	Inversion data set	Control data set 1	Control data set 2
30	2.25	2.78	1.11
45	1.73	3.34	2.60
70	3.58	3.35	2.31
120	4.84	4.74	3.21
All 4 frequencies	3.16	3.51	2.30

Table 8.2: Inversion case 19:3. Fitness values for the inversion data set (receiver depths 20 and 60 m), control data set 1 (receiver depths 10, 50 and 70 m) and control data set 2 (receiver depth 30 m, maybe contaminated by noise, cfr. Sec. 6.6.). Cfr. Tab. 8.1.

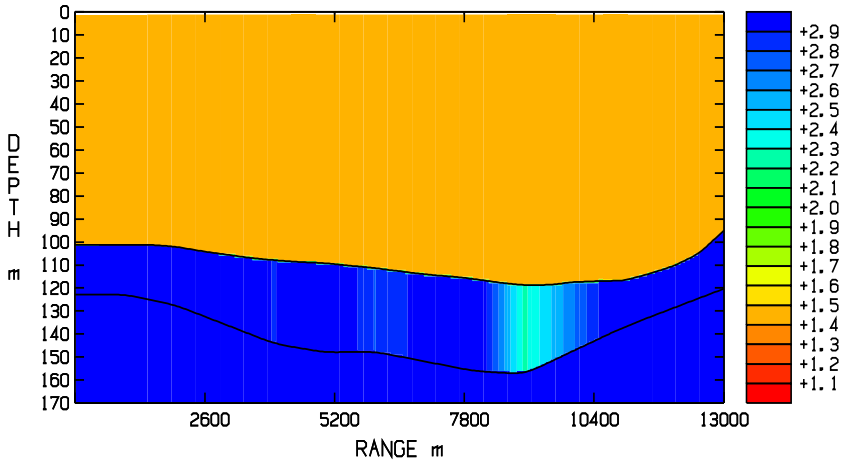

(a) The acoustic impedance (10^6 kg/m^{2}s)

Figure 8.4: The acoustic impedance obtained from inversion 19:3.

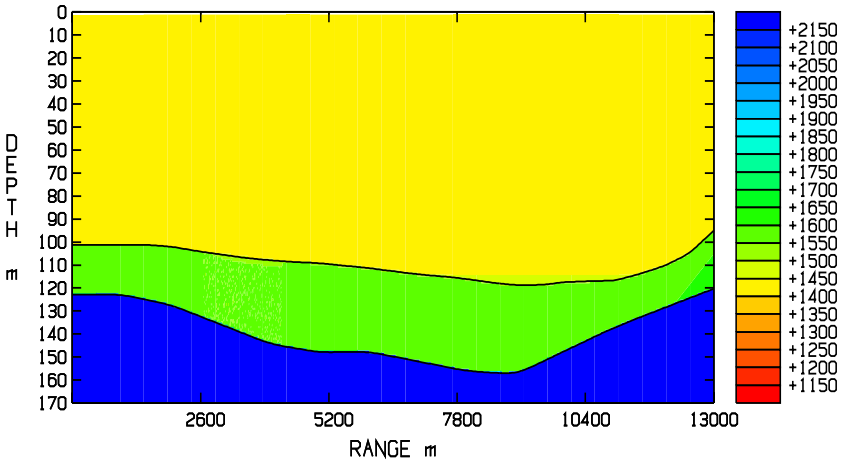

(a) P-velocity (m/s)

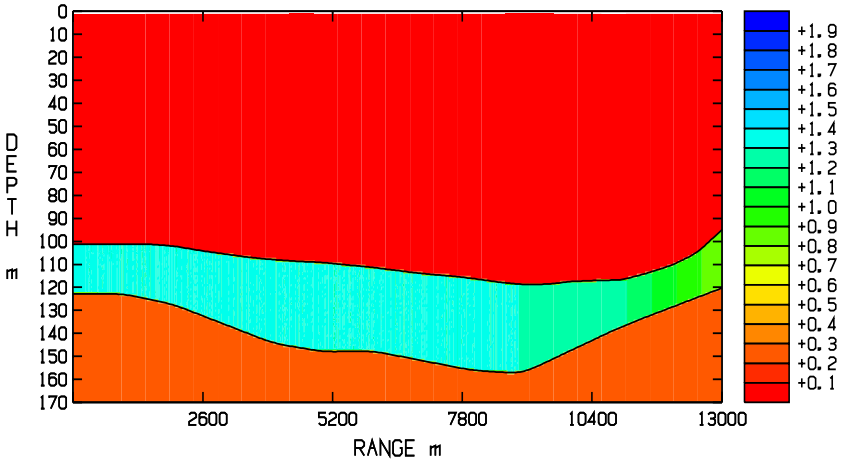

(b) P-attenuation (dB/λ)

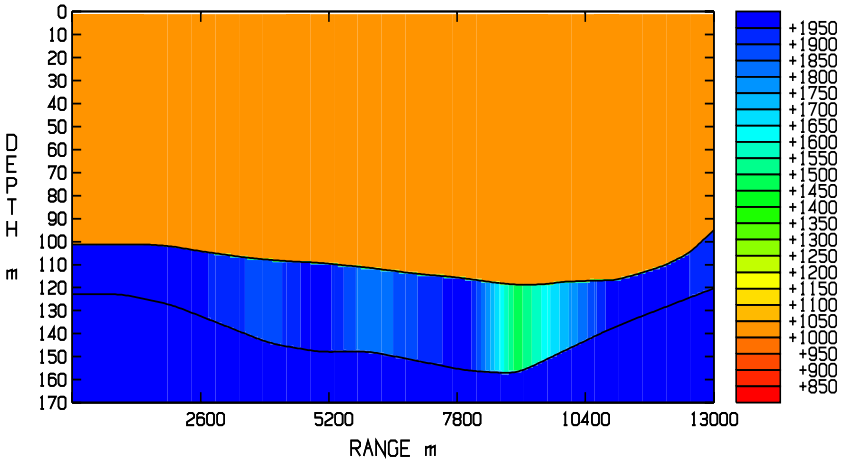

(c) Density (kg/m^3)

Figure 8.5: Media parameters obtained from inversion 19:3.

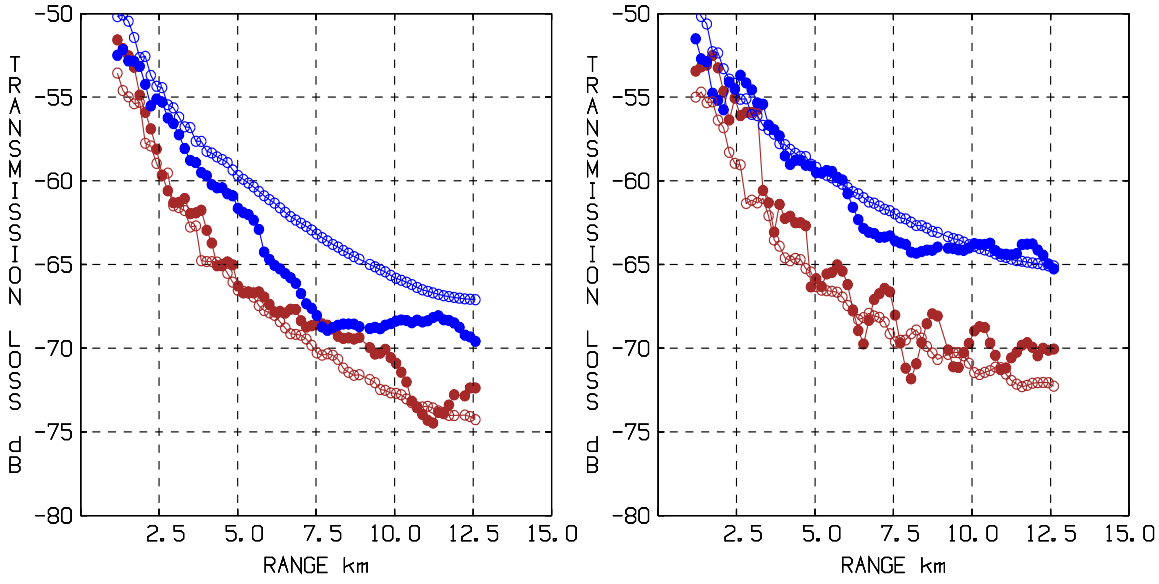

(a) 30 Hz, Fitness = 2.25 dB

(b) 45 Hz, Fitness = 1.73 dB

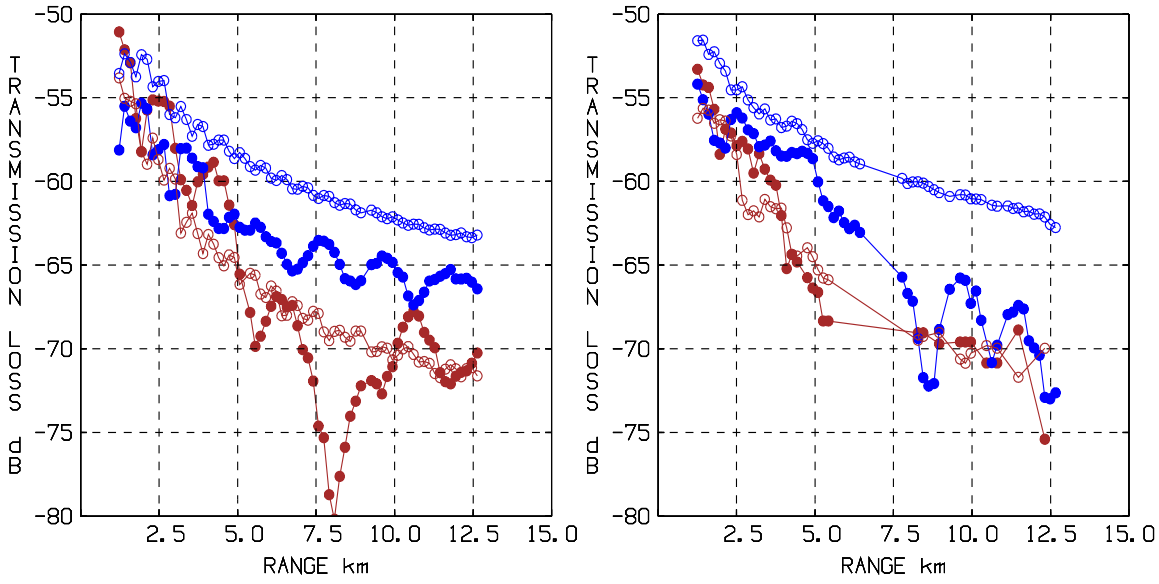

(c) 70 Hz, Fitness = 3.58 dB

(d) 120 Hz, Fitness = 4.84 dB

Figure 8.6: Result of inversion 19:3. Data (filled circles) and model (circles) for receiver depths 20 m (brown) and 60 m (blue).

8.3 Range-dependent fluid seabed with extended search space: Inversion 19:2

Since the GA chose media parameters close to the borders of the search space in inversion 19:3 above (Sec. 8.2), we extended the limits of the search intervals for the sound velocity and attenuation in the present inversion, cfr. Tab. 5.1. The results of the inversion are shown in Figs. 8.8, 8.7 and 8.9. The fitness values for the inversion data set and the control data sets are shown in Tab. 8.3.

By introduction of very low velocities at the beginning of the track, and at ranges from 3 to 7 km the model adjusts to the fast decay of the data in these regions. The resulting match is excellent at all four frequencies, apart from small scale details in the interference patterns of the 45, 70 and 120 Hz cases.

	Fitness [dB]		
Frequency [Hz]	Inversion data set	Control data set 1	Control data set 2
30	1.41	1.79	0.83
45	1.38	2.82	1.56
70	2.58	2.82	3.12
120	2.37	2.79	3.90
All 4 frequencies	1.97	2.58	2.43

Table 8.3: Inversion case 19:2. Fitness values for the inversion data set (receiver depths 20 and 60 m), control data set 1 (receiver depths 10, 50 and 70 m) and control data set 2 (receiver depth 30 m, maybe contaminated by noise, cfr. Sec. 6.6.).

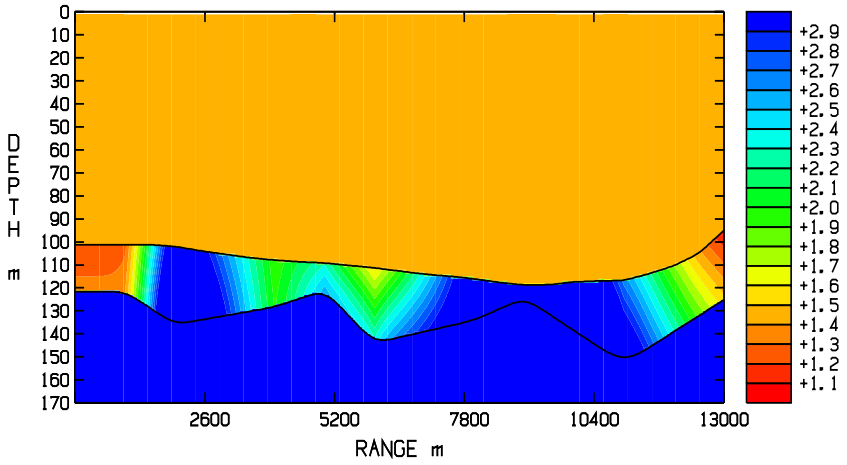

(a) The acoustic impedance (10^6 kg/m^{2}s)

Figure 8.7: The acoustic impedance obtained from inversion 19:2.

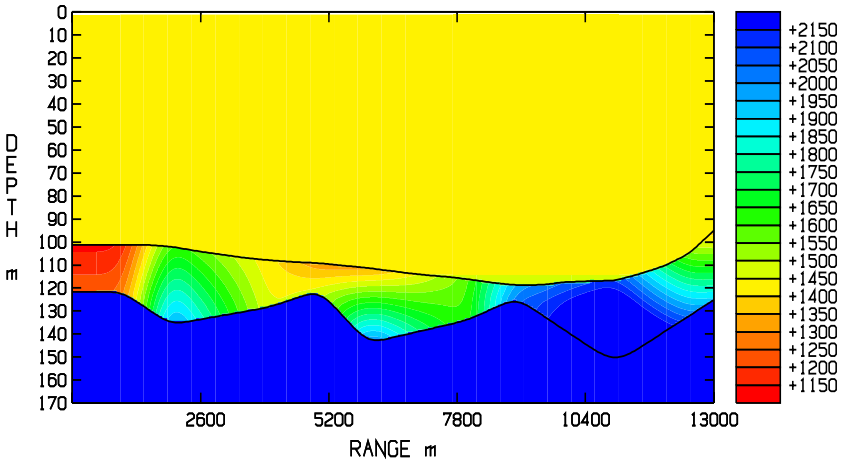

(a) P-velocity (m/s)

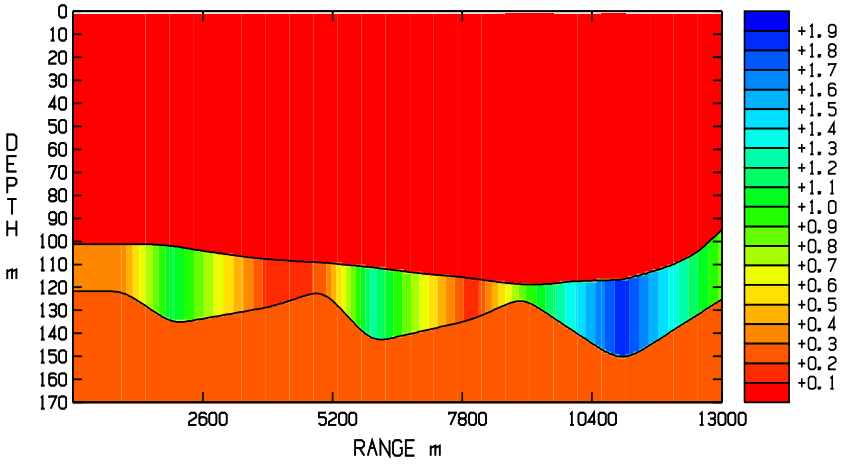

(b) P-attenuation (dB/λ)

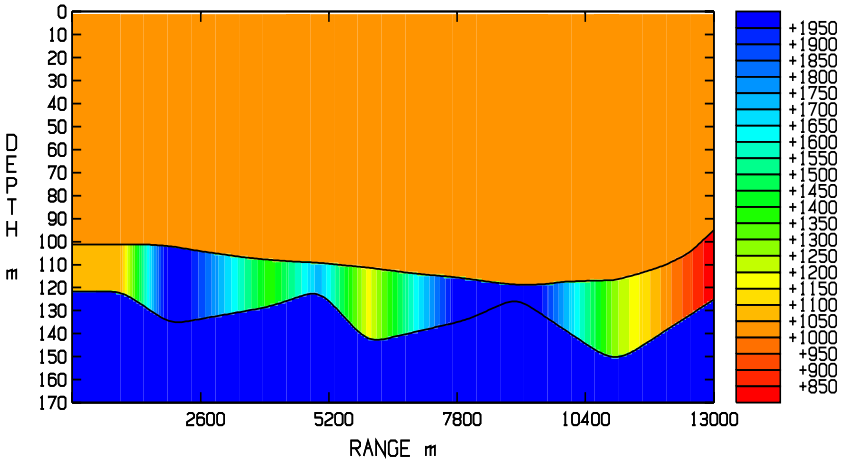

(c) Density (kg/m^3)

Figure 8.8: Media parameters obtained from inversion 19:2.

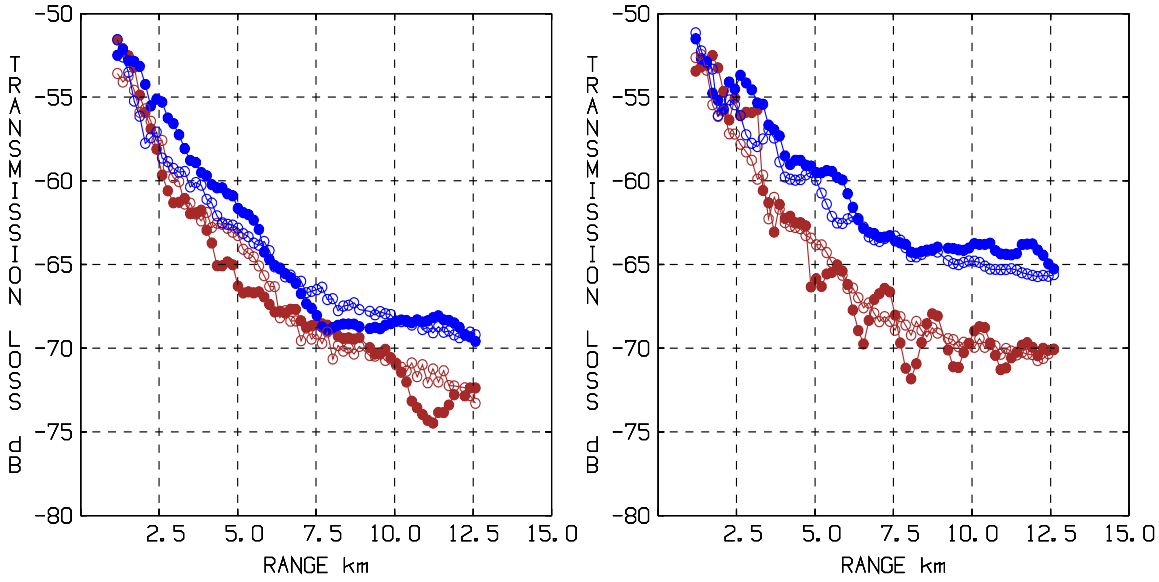

(a) 30 Hz, Fitness = 1.41 dB

(b) 45 Hz, Fitness = 1.38 dB

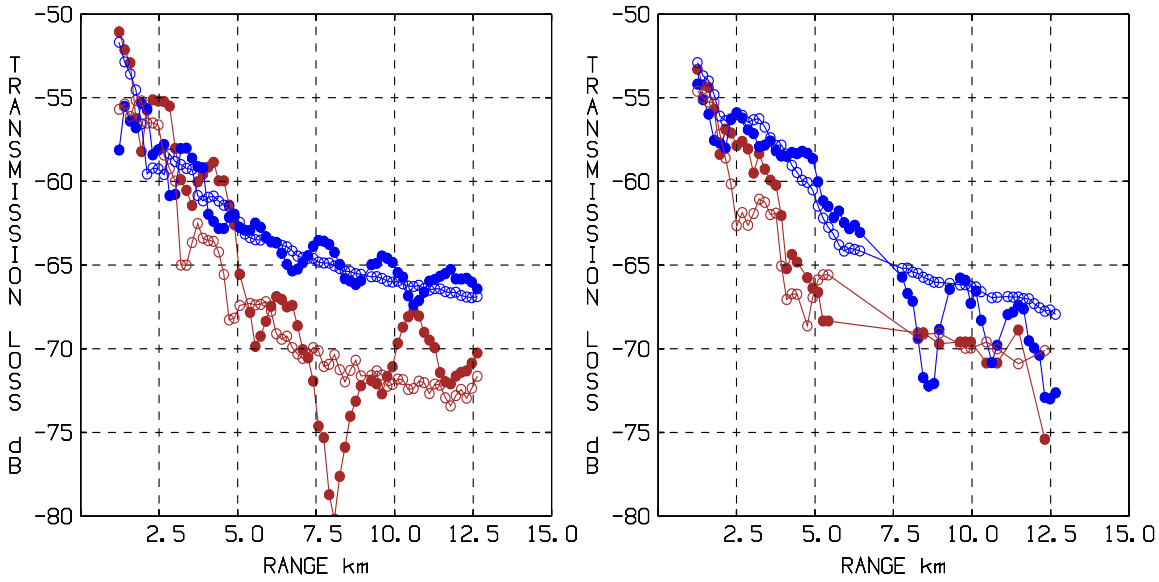

(c) 70 Hz, Fitness = 2.58 dB

(d) 120 Hz, Fitness = 2.37 dB

Figure 8.9: Result of inversion 19:2. Data (filled circles) and model (circles) for receiver depths 20 m (brown) and 60 m (blue).

8.4 Range-independent fluid seabed: Inversion 19:1

See Tab. 5.1 for the search-intervals of the geoacoustic parameters. The result of the inversion is shown in Tab. 8.4 and Fig. 8.10. The fitness values for the inversion data set and the control data sets are shown in Tab. 8.5.

The agreement between model and data is fairly good for this simple model. The mismatch is about 2-3 dB for the three lowest frequencies, about 1 dB higher for 120 Hz.

The GA chose a range-independent model with a very hard bottom in order to match the average decay of the data during the track: In the beginning the decay is fast, in the second half of the track the decay is quite modest. A sensitivity analysis of the media parameters is presented in Sec. 8.4.1.

Water Depth	c_p^{top} [m/s]	c_p^{bot} [m/s]	β_p [dB/λ]	ρ [kg/m^3]	Sediment thickness [m]
90.5	1467	2400	1.49	2107	40.0

Table 8.4: Media parameters obtained from inversion 19:1 with a range-independent fluid seabed. β_p denotes the attenuation, ρ the density, and c_p^{top} and c_p^{bot} the sound velocity at the top and the bottom respectively of the sediment.

	Fitness [dB]		
Frequency [Hz]	Inversion data set	Control data set 1	Control data set 2
30	2.65	3.14	1.03
45	1.99	3.12	2.85
70	3.06	2.81	2.90
120	3.72	3.89	3.64
All 4 frequencies	2.84	3.20	2.64

Table 8.5: Inversion case 19:1. Fitness values for the data set (receiver depths 20 and 60 m), control data set 1 (receiver depths 10, 50 and 70 m) and control data set 2 (receiver depth 30 m, maybe contaminated by noise, cfr. Sec. 6.6.).

8.4.1 Sensitivity analysis

The GA terminated near a minimum of the objective function (red lines). As for the corresponding inversion result 18:1 (Sec. 7.5), the most sensitive parameters are the thickness, the sound velocity and the attenuation of the sediment. However, a wide range of values of these parameters would give almost the same fitness value since the sensitivity curves are very flat around the values chosen by the GA: for example, the thickness is sensitive only for values below 10 m (since the velocity gradient is so high), and the sound velocity is sensitive for values below 1400 m/s only (because of the large value of the density which gives a high impedance contrast and hence total reflection at the water-seabed interface). It is interesting to observe that the GA chose the minimum

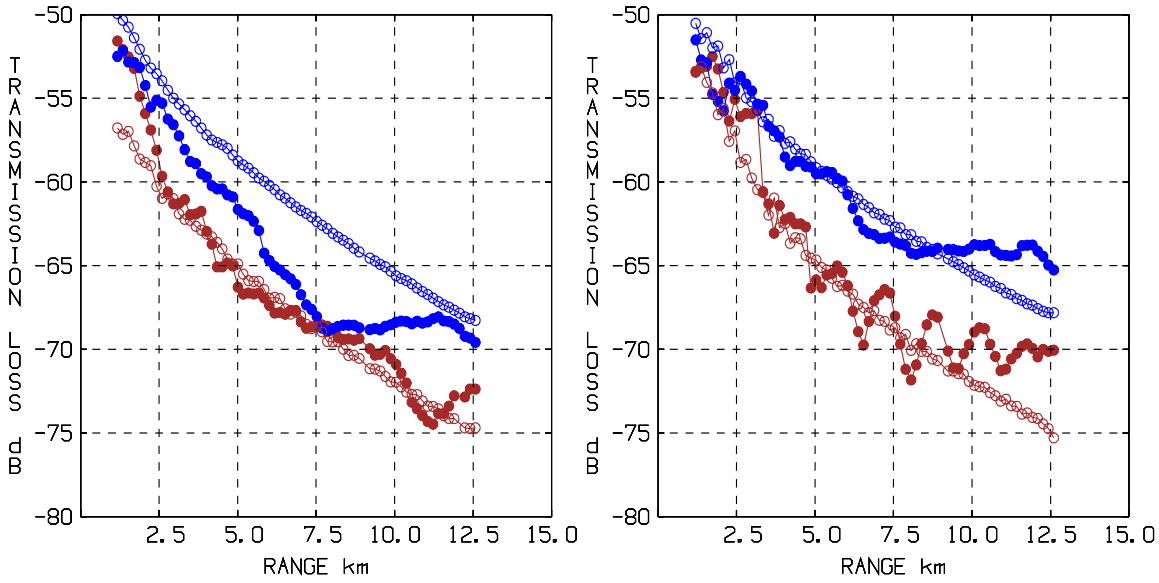

(a) 30 Hz, Fitness = 2.65 dB

(b) 45 Hz, Fitness = 1.99 dB

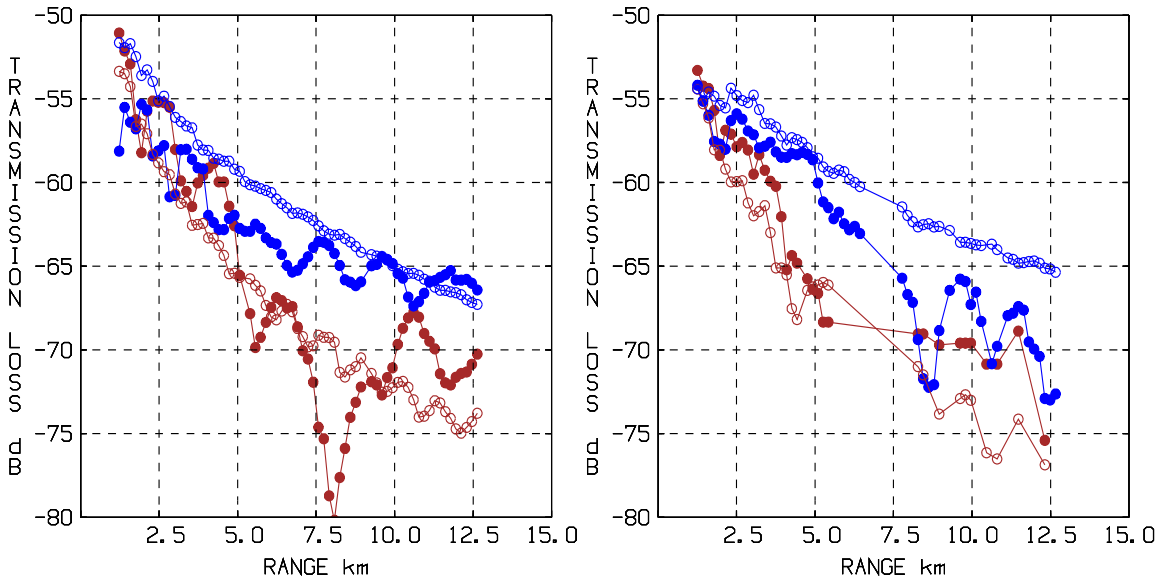

(c) 70 Hz, Fitness = 3.06 dB

(d) 120 Hz, Fitness = 3.72 dB

Figure 8.10: Result of inversion 19:1. Data (filled circles) and model (circles) for receiver depths 20 m (brown) and 60 m (blue).

allowed value of the water depth (90 m), which is smaller than the minimum water depth along the track (varies between 95 and 120 m, cfr. Fig. 2.2). The water depth would probably have been reduced further if the search interval had been wider, cfr. Fig. 8.11. The reason for this is most probably that the model tries to compensate for the small decay of the data in the second half of the track by shrinking the water volume in order to minimize the geometrical spreading of the sound.

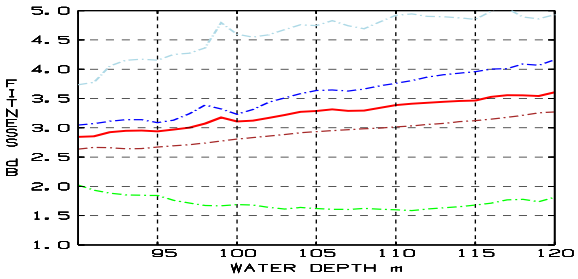

(a) Fitness as function of water depth.

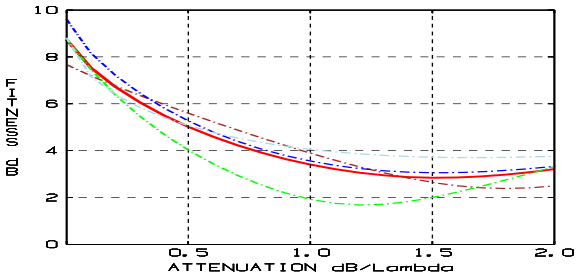

(b) Fitness as function of attenuation.

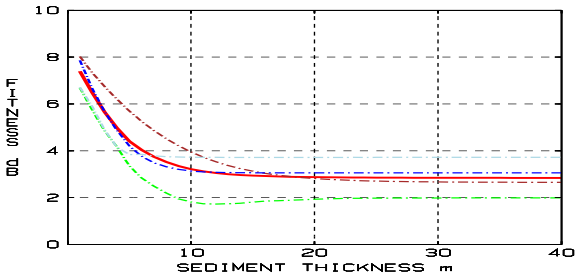

(c) Fitness as function of sediment thickness.

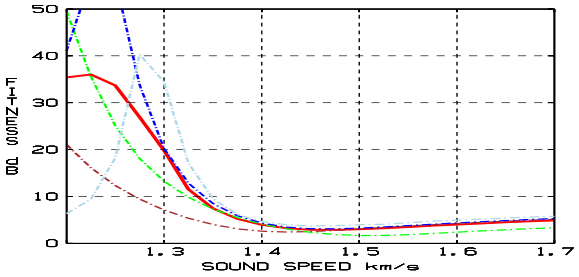

(d) Fitness as function of sound velocity at the top of the sediment.

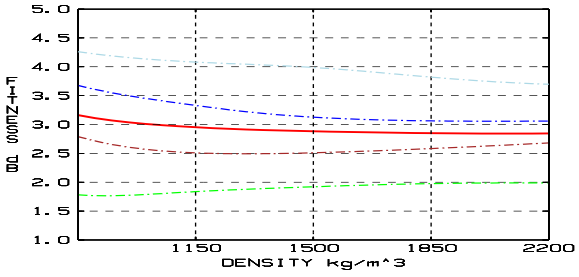

(e) Fitness as function of density.

Figure 8.11: Variation of the fitness value as the parameters of inversion 19:1 are varied. Fitness based on all four frequencies (red line), on data for 30 Hz (brown), 45 Hz (green), 70 Hz (blue) and 120 Hz (light blue).

9 Concluding remarks

In this report low-frequency transmission loss data (30-120 Hz) from a test site east of Gotland have been analyzed. The experimental data were recorded during the last day of the BAROC (Baltic Acoustics on Rocky Out Crops) field trial in May 2002, which was a joint work between FOI and FWG (Forschungsanstalt der Bundeswehr für Wasserschall und Geophysik, Kiel, Germany). The water depth at the site was about 100 metres, with a seabed composed of 5 to 20 m sediments of clayey silt and moraine above limestone bedrock.

The recordings were made along two tracks, and the propagation characteristics of the sound differed considerably between these: along the north-east track (Run 18) the sound was lost in the background noise already after 5-7.5 km, while along the east direction (Run 19) the signals were well above the ambient noise level still at the end of the run at 13 km.

The objectives of the analysis were, first, to investigate how well the TL data could be reproduced by a numerical sound propagation model by adjusting the unknown parameters and geometry of the seabed so as to minimize the model-data mismatch. Second, to compare the resulting 'acoustically equivalent' seabed model with what is known about the geological structure of the seabed in this area. Third, to compare the modeling capabilities of environmental models of different degrees of complexity.

It turned out that already the simplest possible model, a horizontally stratified fluid seabed model, managed to reproduce the TL data with a mismatch of the order of 3 dB. This is not surprising since the seabed is almost flat at the trial site, the slope of the seabed nowhere exceeds one degree along the tracks. However, by allowing the media parameters to vary with range, the mismatch could be reduced further with up to 1 dB. In fact, further improvement of the match is not meaningful because of the uncertainties in the data.

The range-dependent seabed models obtained from the inversions were of two fundamentally different types: on one hand a solid seabed with media parameters close to the 'ground truth', on the other a fluid seabed with media parameters which diverged from the 'ground truth'. Both types of models managed to reproduce the data. In fact, along the less lossy track 19 the simpler fluid model gave the best match. It looks like the fluid model compensates for the absence of loss-mechanisms due to shear waves by choosing unrealistically low values of the sound velocity (down to 1100 m/s) in the seabed. This need not be a severe drawback, since the primary purpose of the models is to predict the sound propagation in the water column. However, a model close to the 'ground truth' is likely to produce more reliable predictions with respect to seasonal variations of the water level and the sound velocity profile.

The significance of the shear parameters increases with increasing loss of the sound into the seabed. The model-data mismatch along the lossy track 18 with media parameters

close to the 'ground truth' increased by about 2 dB when the shear parameters were removed, but only with about 0.5-1 dB along the less lossy track 19. The modest variations with range of the sound velocity in the water had no effect on the wave propagation at these low frequencies.

A comparison between two different ways of defining the fitness function was carried out. The first measured the mismatch in absolute sound level, the second the mismatch of the relative decay of the TL only. The result indicated that the latter works well and can be an alternative when the source and/or receivers are not well calibrated or the numerical model has problems to reproduce the correct sound level.

A drawback of the analysis has been the absence of a control data set of frequencies not involved in the inversion. We have only tested the results against data in the hydrophones which not took part in the inversion. During the BAROC trial in May 2002 TL from transmitted FM-pulses in the frequency range 350-6000 Hz were also recorded along the same tracks. These data have not yet been analyzed. In future work they should be incorporated in the inversions too, and then TL data from intermediary frequencies should be used as control data. This would serve as a better ground for assessing environmental models which are close to or far from the expected 'ground truth'.

Finally, an issue which should be payed regard to in future work is how dense the data points need to be sampled for estimating a smoothed level of the TL stably with respect to uncertainties in the positions of the data. In this work the distances between the data points were of the order 150-200 m, while the wavelengths were of the order 10-50 m. An example showed that uncertainties in the position of the order of 5-50 m could result in differences in the computed smoothed TL-level of up to 6-7 dB at certain points.

10 Acknowledgement

First of all we would like to thank Dr. Lothar Ginzkey and Dr. Wolfgang Jans at FWG for kindly having provided us with calibration curves for the receiver hydrophones and for helping us when we were puzzled concerning the recorded sound levels.

We would also like to thank the following colleagues at FOI:

Jörgen Pihl, Eva Dalberg, Gunnar Sundin, Örjan Staaf and Per Morén for valuable discussions about different aspects of the Baroc trial. Per Söderberg for providing valuable geological information about the test site. Robert Sigg for providing us with the range-dependent sound velocity profiles recorded during the trial. Torbjörn Ståhlsten and Lars Lekzén for discussions concerning calibration of transmitters and hydrophones. Mika Levonen for discussions concerning the ambient noise levels in the Baltic. Leif Abrahamsson for valuable discussions concerning the numerical modeling. Jan-Olof Hegethorn and Eva Norrbrand for helping us to scan the map over the test site area

and put it in a form that could be used in this report.

References

[1] B.L. Andersson. JEPE-S, a PE code for wave propagation in range-dependent fluid-solid media. Technical report FOA-R–98-00979-409–SE, 1998.

[2] A. Sundström. A stable PE model for wave propagation in fluid-solid media. Scientific report FOA-R-00-01741-409–SE, 2000.

[3] M. Sambridge and G. Drijkoningen. Genetic algorithms in seismic waveform inversion. *Geophys. J. Int.*, 109:323–342, 1992.

[4] T. Flodén. Seismic stratigraphy and bedrock geology of the central Baltic. Acta Universitatis Stockholmiensis, Stockholm contributions in geology, Vol. XXXV, 1980.

[5] P. Söderberg. Seismic stratigraphy, tectonics and gas migration in the Åland Sea, northern Baltic Proper. Acta Universitatis Stockholmiensis, Stockholm contributions in geology, 43 (1), 1993.

[6] L.-Z. Gelumbauskaité, T. Holmquist, V. Litvin, B. Malkov, S. Seredenko, O. Stiebrins, and Sz. Uścinowicz. *Bathymetric map of the central Baltic Sea, scale 1:1500000.* LGT Series of Marine Geological Maps/SGU Series Ba no. 54 Vilnius-Uppsala., 1998.

[7] S. Ivansson and I. Karasalo. A high-order adaptive integration method for wave propagation in range-independent fluid-solid media. *J. Acoust. Soc. Amer.*, 92:1569–1577, 1992.

[8] I. Karasalo. Exact finite elements for wave-propagation in range-independent fluid-solid media. *J. Sound Vib.*, 172:671–688, 1994.

[9] E.Parastates. Narrowband MFP of shallow water experimental data. Scientific report FOA-R–99-01284-409–SE, 1999.

[10] D. Whitley and T. Starkweather. GENITOR II: a distributed genetic algorithm. *J. Expt. Theor. Artif. Intell.*, 2:189–214, 1990.

[11] R. Jeltsch. Multistep methods using higher derivatives and damping at infinity. *Math. Comp.*, 31:124–138, 1977.

[12] F.B. Jensen, W.A. Kuperman, M.B. Porter, and H. Schmidt. *Computational Ocean Acoustics.* AIP Press, New York, 1994.

[13] L. Abrahamsson, B.L. Andersson, I. Karasalo, and P. Sigray. Environment assessment for underwater sensors in the Stockholm archipelago, Part 1 - Inversion of hydroacoustic sub-bottom parameters. User report FOI-R–0706–SE, 2002.

[14] Y.C.Fung. *Foundations of solid mechanics.* Prentice-Hall, Inc., New Yersey, 1965.

[15] P.G.Richards K.Aki. *Quantitative seismology, vol. 1.* W.H. Freeman and company, San Francisco, 1980.